

OAK RIDGE NATIONAL LABORATORY
CENTRAL RESEARCH LIBRARY
DOCUMENT COLLECTION

LIBRARY LOAN COPY

DO NOT TRANSFER TO ANOTHER PERSON

If you wish someone else to see this
document, send in name with document
and the library will arrange a loan.

UCN-7969
(3-3-67)

CENTRAL RESEARCH LIBRARY
DOCUMENT COLLECTION

LOCKHEED MARTIN ENERGY RESEARCH LIBRARIES



3 4456 0515551 4

1

ORNL-4369

UC-25 - Metals, Ceramics, and Materials

RADIATION METALLURGY SECTION

SOLID STATE DIVISION

PROGRESS REPORT

FOR PERIOD ENDING OCTOBER 1968



OAK RIDGE NATIONAL LABORATORY

operated by

UNION CARBIDE CORPORATION

for the

U.S. ATOMIC ENERGY COMMISSION

Printed in the United States of America. Available from Clearinghouse for Federal
Scientific and Technical Information, National Bureau of Standards,
U.S. Department of Commerce, Springfield, Virginia 22151
Price: Printed Copy \$3.00; Microfiche \$0.65

LEGAL NOTICE

This report was prepared as an account of Government sponsored work. Neither the United States, nor the Commission, nor any person acting on behalf of the Commission:

- A. Makes any warranty or representation, expressed or implied, with respect to the accuracy, completeness, or usefulness of the information contained in this report, or that the use of any information, apparatus, method, or process disclosed in this report may not infringe privately owned rights; or
- B. Assumes any liabilities with respect to the use of, or for damages resulting from the use of any information, apparatus, method, or process disclosed in this report.

As used in the above, "person acting on behalf of the Commission" includes any employee or contractor of the Commission, or employee of such contractor, to the extent that such employee or contractor of the Commission, or employee of such contractor prepares, disseminates, or provides access to, any information pursuant to his employment or contract with the Commission, or his employment with such contractor.

ORNL-4369

Contract No. W-7405-eng-26

RADIATION METALLURGY SECTION
SOLID STATE DIVISION
PROGRESS REPORT
For Period Ending October 1968

M. S. Wechsler, Head, Radiation Metallurgy Section
Solid State Division

APRIL 1969

OAK RIDGE NATIONAL LABORATORY
Oak Ridge, Tennessee
Operated by
UNION CARBIDE CORPORATION
for the
U. S. ATOMIC ENERGY COMMISSION

LOCKHEED MARTIN ENERGY RESEARCH LIBRARIES



3 4456 0515551 4

Reports previously issued in this series are as follows:

ORNL-3878	Period Ending August 1965
ORNL-3949	Period Ending February 1966
ORNL-4020	Period Ending July 1966
ORNL-4097	Period Ending January 1967
ORNL-4195	Period Ending July 1967
ORNL-4246	Period Ending January 1968
ORNL-4334	Period Ending July 1968

CONTENTS

Summary	iv
Radiation Effects in Alloys and Structural Materials	1
Radiation Effects on Pressure-Vessel Steels	1
Radiation Hardening and Embrittlement in ASTM A 212-B Steel	1
Electron Fractography of Irradiated A 212-B Pressure-Vessel Steel	9
Radiation Hardening and Embrittlement in ASTM A 533-B Steel	16
Properties of 12-in.-Thick ASTM A 533-B Class 1 and Class 2 Steels	21
Radiation Effects in Iron	29
Radiation Hardening in Iron	29
Radiation Effects in Vanadium.	42
Trapping of Interstitial Impurities in Vanadium Defects Produced by Radiation	42

SUMMARY

Several new techniques have now been employed in our study of the radiation hardening and embrittlement of reactor pressure-vessel steels. The impact machines in the laboratory and hot cell have been fitted with strain gages whose calibrated output registers the load applied to the sample during impact. The total energy to fracture determined from the strain-gage output agrees with that indicated on the scale of the impact machine. The general yield load, the maximum load, and the fracture load were evaluated as a function of test temperature for unirradiated A 212-B and A 533-B steel and for A 533-B steel irradiated at three temperatures. The temperature at which the general yield load curve intersects the maximum or fracture load curve appears to correlate well with the ductile-to-brittle transition temperature (DBTT) determined on a zero-fracture-energy criterion.

Unirradiated and irradiated steels have been observed by optical and electron microscopy including electron fractography by replication of the fracture surfaces. No major difference in appearance of the unirradiated and irradiated material has been detected. Thin foils of unirradiated and irradiated steel specimens were examined by transmission electron microscopy; the irradiated foils showed no evidence of defect clusters produced by radiation, although the exposure was sufficient to cause significant hardening and embrittlement.

In conjunction with the Heavy Section Steel Technology Program, we conducted impact and tensile tests on irradiated specimens from HSST plate 01, a 12-in.-thick plate of A 533-B steel. In comparison with other steels of the same general type, this steel displayed an intermediate degree of radiation-embrittlement sensitivity. We also performed impact and tensile tests on unirradiated specimens of several orientations taken from several depths in HSST plate 02. Specimens from the surface of the plate exhibited the lowest DBTT, and specimens of longitudinal orientation showed the greatest ductile fracture energy.

Three aspects of radiation hardening in Fe are described: temperature dependence, fluence dependence, and the effect of interstitial solutes. After a low-fluence irradiation (1×10^{16} neutrons/cm²), the yield stress of vacuum-melted Fe is increased about the same amount

at all test temperatures; but after a higher-fluence irradiation (3×10^{19} neutrons/cm²), the yield stress increase is larger at lower test temperatures. When the radiation hardening of several irons was analyzed on the basis of a square-root dependence on the fluence, the rate of hardening was found to decrease with increasing exposure. The amount of hardening was greater in samples with higher carbon concentrations. The effect of nitrogen content was studied in samples containing less than 1 and about 20 ppm N by weight irradiated below -50°C , where N is immobile. Upon postirradiation annealing to 250°C , the rate of radiation-anneal hardening was about the same for the Fe and Fe-20N materials. However, the magnitudes of the increase in flow stress and the drop in yield upon strain aging decreased sharply for Fe-20N annealed at 100°C , indicating that N is removed from solid solution by becoming trapped at defects produced by radiation.

Finally, measurements of resistivity and internal friction have been made on irradiated V. The results are similar to those for irradiated Nb in indicating that interstitial impurities (O and N) migrate to traps produced by radiation and are thus effectively removed from solid solution.



RADIATION EFFECTS IN ALLOYS AND STRUCTURAL MATERIALS

M. S. Wechsler

The object of this program is to investigate the underlying causes of the embrittlement of metals and structural alloys by radiation. Because of the critical importance of reactor pressure vessels, the program is particularly concerned with reactor irradiation effects in Fe and pressure-vessel steels.

The materials under study are base metal, heat-affected zones, and the weld metal in the commercial ASTM pressure-vessel alloys such as A 212-B, A 302-B, A 533-B, and A 543. The variables being investigated are material history, composition, the irradiation neutron flux and spectrum, and the irradiation temperature.

To enlarge the understanding of the effects produced by the interaction of the irradiation-induced defects and impurities in the commercial steels, we include studies of the effects of irradiation on Fe and V.

Radiation Effects on Pressure-Vessel Steels

Radiation Hardening and Embrittlement in ASTM A 212-B Steel (N. E. Hinkle, R. G. Berggren, W. J. Stelzman, T. N. Jones, M. S. Wechsler, and C. R. Case II¹)

In a previous report² we described an attempt to relate radiation hardening, as determined by measurements of tensile yield and fracture stress, to radiation embrittlement exhibited by Charpy notch-impact specimens of ASTM A 212-B pressure-vessel steel. Through the use of an estimated correction of strain rate, a calculated triaxiality factor,³

¹Summer Trainee from University of Wisconsin, Oshkosh, Wisconsin, sponsored by Oak Ridge Associated Universities.

²M. S. Wechsler, N. E. Hinkle, R. G. Berggren, and W. J. Stelzman, Radiation Metallurgy Section Solid State Division Progress Report for Period Ending January 1968, ORNL-4246, pp. 6-27.

³T. R. Wilshaw and P. L. Pratt, "The Effect of Temperature and Strain Rate on the Deformation and Fracture of Mild-Steel Charpy Samples," pp. 973-991 in Proceedings First International Conference on Fracture, Vol. 2, The Japanese Society for Strength and Fracture of Materials, Japan, 1966.

and the assumption of a cleavage fracture load independent of temperature and strain rate, we found that the radiation hardening was more than sufficient to cause the observed shift in ductile-to-brittle transition temperature (DBTT). In order to define this relationship more precisely, we have extended our investigation of the effect of strain rate on yielding and fracture in the notched specimens. To do this, it was necessary to obtain quantitative measurements of the load applied to Charpy notched-bar specimens as a function of strain rate and temperature. Two approaches were taken to measure the loads applied to the notched-bar samples. First, the strikers of the impact machines were fitted with strain sensors whose outputs were calibrated to yield the loads applied to the samples during the impact test. Second, slow-bend tests were performed at a low strain rate on the notched-bar samples loaded in three-point bending. The loads were measured in an Instron machine in tests conducted as a function of temperature in a test chamber cooled by liquid N. To elucidate the strain pattern near the root of the notch, we attempted to reveal yield zones by etching.

Although most of our earlier work has been devoted to the ASTM A 212-B steel, our studies have now been extended to include ASTM A 533-B pressure-vessel steel. This is described in another section of this report.⁴

The information that can be determined from a standard impact test includes the total energy to fracture, fracture appearance, and lateral expansion and contraction; but no details of the deformation during the test are provided. Wilshaw and Pratt,³ Fearneough and Hoy,⁵ and Tetelman and McEvily⁶ have shown that the load and energy absorbed by a Charpy notch-impact specimen can be determined at any time during the test with an impact machine instrumented with strain sensors. We believe

⁴R. G. Berggren et al., "Radiation Hardening and Embrittlement in ASTM A 533-B Steel," pp. 189-194, this report.

⁵G. D. Fearneough and C. J. Hoy, J. Iron Steel Inst. (London) 202, 912-920 (November 1964).

⁶A. S. Tetelman and A. J. McEvily, Jr., Fracture of Structural Materials, pp. 322-325, Wiley, New York, 1967.

that the instrumented Charpy impact test provides a favorable tool for studying the relationship between radiation hardening and embrittlement.

We have completed the instrumentation of two impact machines, one for use in a hot cell and one for use in the laboratory. The laboratory machine was equipped with a strain-gage bridge network consisting of a pair of Baldwin-Lima-Hamilton foil strain gages (type FAE-50-35S6, 0.5-in. gage length). These were placed in recesses on the sides of the Charpy striker along the center of the impact to serve as the active bridge element. A pair of identical gages for temperature compensation, located on the striker flange, served as the inactive bridge elements.

The impact machine used in the hot cell has a pair of Budd He-121-R2TC strain gages placed in recesses on the sides of the striker. These are high-elongation, rosette foil gages with a two-element 90° rectangular grid of 1/8-in. gage length. They are oriented to provide strain measurements parallel and normal to the direction of impact. All four sensor elements are active in this bridge network.

A Tektronix Model 543 oscilloscope, equipped with a Type Q plug-in module, provides the alternating-current excitation voltage for the strain-gage bridge. The output voltage of the bridge network is displayed on the oscilloscope screen. The oscilloscope has a single-sweep internal triggering mode that is armed manually as the pendulum descends at the start of a test. The oscilloscope traces are photographed with a Polaroid camera (see Fig. 1).

Both systems were calibrated statically for load on an Instron tensile machine. The load was applied to the striker via a standard Charpy notch-impact specimen properly positioned at the point of contact at the leading edge of the striker. The strain in the striker, as detected by the strain gages and traced on the oscilloscope screen, is directly proportional to the applied load, which is detected by the load cell of the tensile machine and graphically displayed on a strip-chart recorder. As an indication of the reliability of the oscilloscope traces and the load calibration, the fracture energies of a series of tests have been derived from the traces. These are compared in Fig. 2 with the fracture energies obtained from the scale on the impact machine.

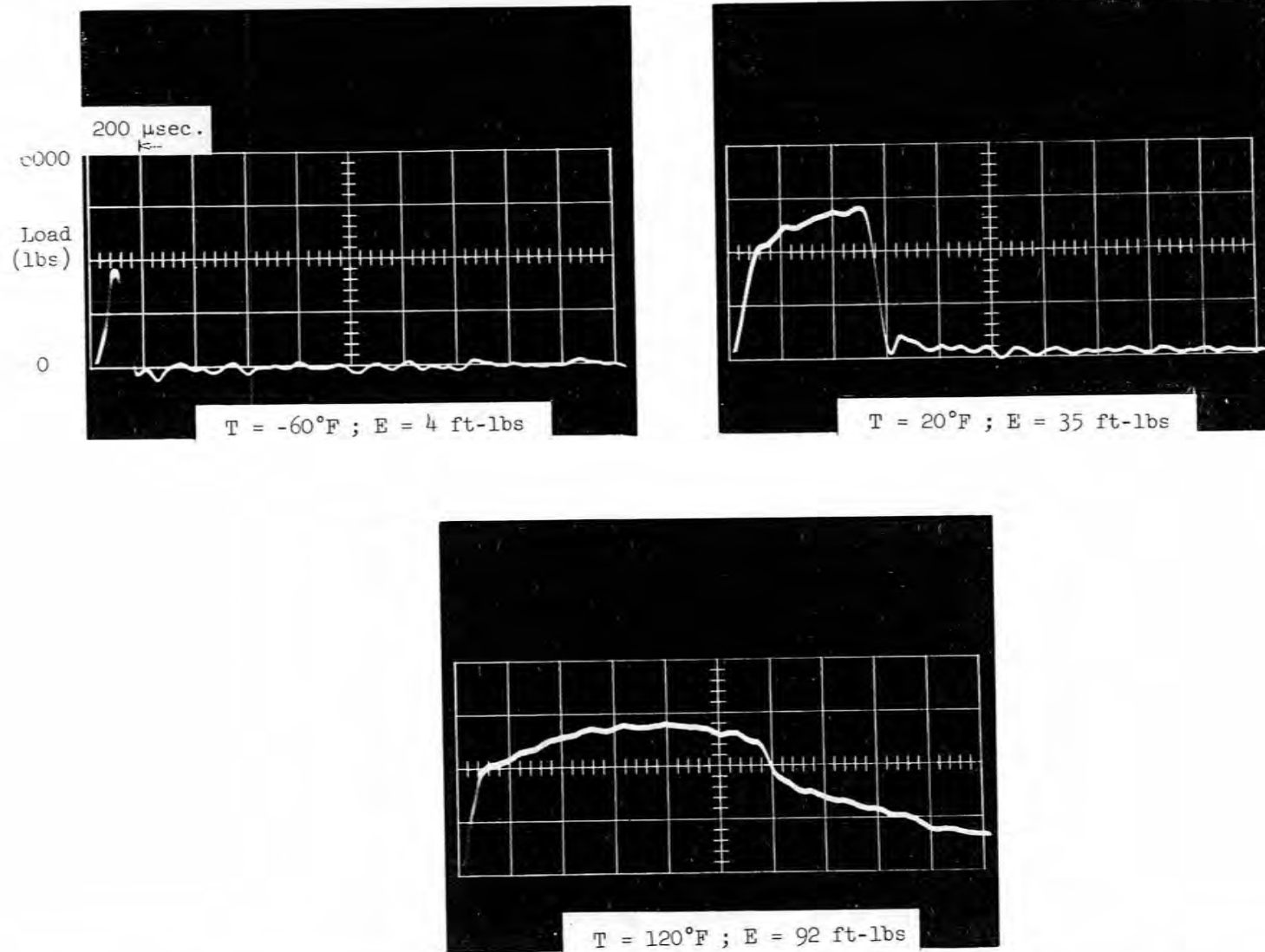


Fig. 1. Oscilloscope Traces of the Output of the Strain Gages Mounted on the Striker of the Impact Machine.

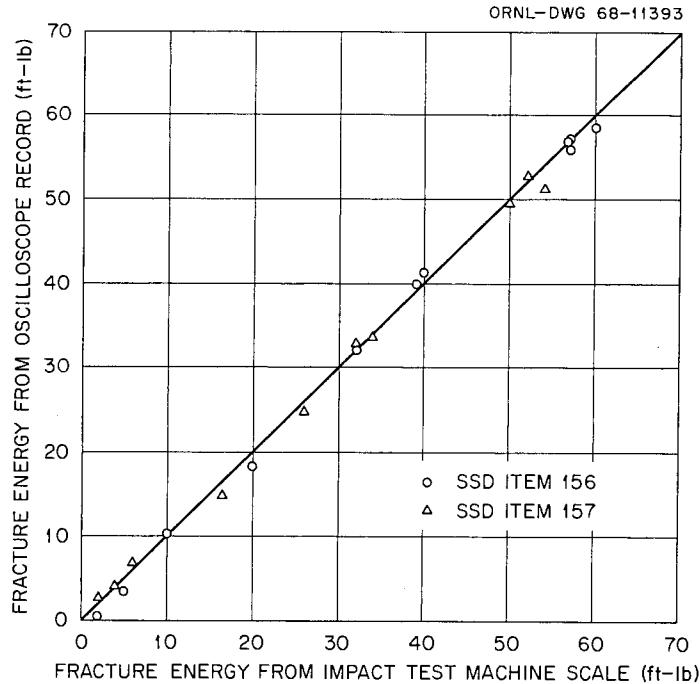


Fig. 2. Comparison of the Fracture Energy Measured by the Impact Machine with the Fracture Energy Calculated from the Oscilloscope Traces.

Charpy notch-impact specimens were also bend tested at low strain rate in a three-point-bend test apparatus mounted on an Instron tensile machine. The sample holder for the bend tests has the same shape as the anvil and striker of the impact machine.

The general yield load and fracture load for the impact tests on the A 212-B steel (Solid State Division Item 156) as measured with the strain-gage instrumentation are shown as a function of temperature in Fig. 3 (open and closed squares, respectively). The corresponding quantities for the slow-bend tests as measured on the tensile machine are also shown (open and closed circles, respectively). We see that the curves for impact tests are shifted about 150°C upward on the temperature scale with respect to the curves for slow-bend tests. The fracture load curves for impact and slow-bend tests have a similar shape, but the general yield curve for slow-bend tests appears to decrease more rapidly with increasing temperature than that for the impact tests.

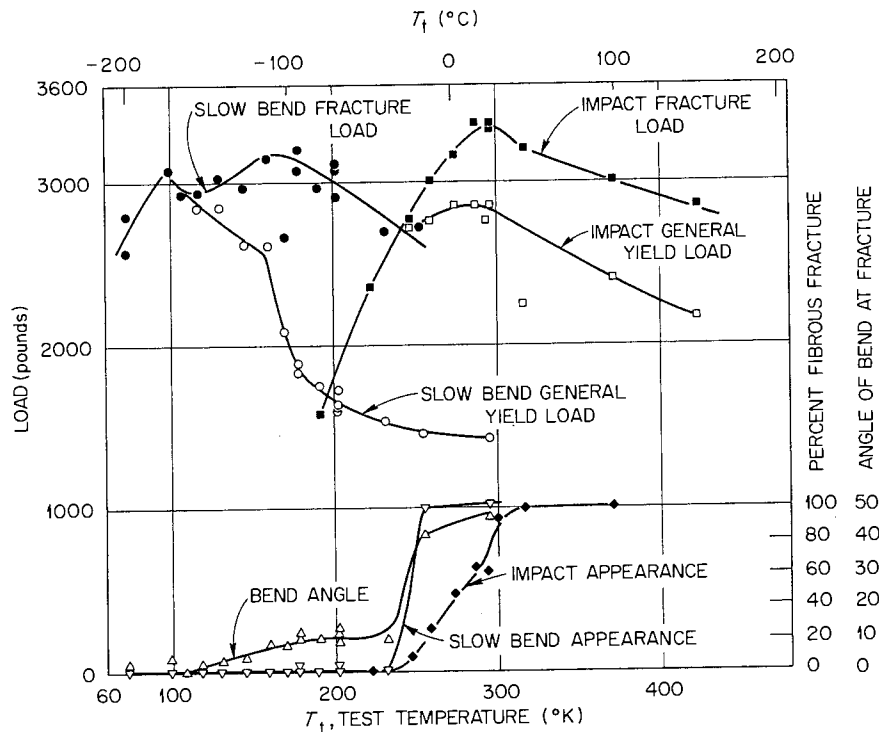


Fig. 3. The General Yield Load and Fracture Load from Impact and Slow-Bend Tests as a Function of Test Temperature. Also shown are the percent fibrous-fracture appearance for impact and slow-bend tests and the bend angle at fracture for the slow-bend tests. Unirradiated Charpy V-notch samples of A 212-B steel, SSD Item 156.

In the earlier work,⁷ the criterion used for the critical cleavage stress, σ_c , was the point of intersection of the yield and fracture stresses as determined from tensile tests at low strain rates on smooth samples. The σ_c thus determined was assumed to be independent of strain rate. Applying this criterion to the results of the notched-bar tests in Fig. 3, we find the σ_c for slow bend to correspond to a load of about 2900 lb (at 110 K) and for impact tests, 2750 lb (at 240 K). Thus, the σ_c does indeed appear to be quite insensitive to strain rate.

⁷M. S. Wechsler, N. E. Hinkle, R. G. Berggren, and W. J. Stelzman, Radiation Metallurgy Section Solid State Division Progress Report for Period Ending January 1968, ORNL-4246, pp. 6-27.

The fracture surfaces of the impact and slow-bend specimens appeared somewhat different, probably due to the differences in strain rate and temperature. At temperatures just above the DBTT, the fracture surface of the impact specimen has the usual crystalline appearance (indicative of cleavage fracture) at the center, surrounded by a border of fibrous appearance (indicative of shear fracture) at the edges of the fracture surface. The slow-bend specimens, on the other hand, show fibrous-fracture appearance only near the root of the notch, with the crystalline appearance extending completely to the other three edges of the fracture surface.

As shown in Fig. 3, the change in the appearance of the fracture surface of impact specimens from 100% fibrous to 100% crystalline occurs in the temperature range where the impact fracture load reaches a maximum and the impact general yield load intersects the fracture load [i.e., from 295 K (22°C) to 250 K (-23°C)]. The DBTT determined by the impact energy criterion occurs in the same temperature range as that determined by the change in fracture appearance. Thus, the percent of fibrous-fracture appearance correlates with both the impact energy transition and the intersection of the curves of yield and fracture loads. However, the fracture-appearance transition of the slow-bend specimens, which occurs between 230 K (-43°C) and 255 K (-18°C), does not match the DBTT indicated by the intersection of the curves for slow-bend general yield and fracture load at 110 K (-163°C). These results indicate that the fracture appearance is not a positive indicator of the DBTT for tests of Charpy notch-impact specimens at low strain rates.

Figure 3 also shows the bend angles of the slow-bend specimens at fracture. The bend angle increases slowly from 0° near 110 K (-163°C), where the curves for general yield and fracture load intersect, to about 10° at the fracture-appearance transition temperature, 230 K (-43°C). The energy of deformation during slow bend has been calculated, and, as with the bend angle, it also increases gradually from near 110 K to about 230 K, where gross shear deformation becomes the controlling mechanism.

In summary, if the DBTT is defined as that temperature at which the fibrous-fracture appearance is essentially zero,^{7,8} this is seen to be the temperature at which curves for the impact general yield and fracture loads intersect. For the slow-bend tests, however, this criterion is not applicable. We find instead that the DBTT of slow-bend tests is better defined by a bend angle of 0° at fracture.

In our previous work on the relationship between radiation hardening and embrittlement,^{7,8} we also found that the DBTT of the irradiated impact specimens could be predicted from the tensile results if it were assumed that the maximum triaxiality correction factor,⁹ used to obtain reasonably good agreement for unirradiated specimens, was reduced as a result of the irradiation. A decrease in the maximum triaxiality correction factor implies that the plastic zone, developed at the root of the notch before cleavage fracture is initiated, has been decreased. Using notch-impact specimens of A 212-B (Solid State Division Item 156) and the slow-bend technique, we attempted to study the development of the plastic zone at the root of the notch. Specimens were subjected to various loads up to the fracture or general yield loads near the DBTT and then etched to reveal the plastic zone and the development of the plastic hinges. We found it relatively easy to see the plastic hinges at the general yield load without etching, but at the lower stresses we were unable to observe the development of the plastic zone at the root of the notch even after using variations of Fry's reagent with or without thermal aging. Apparently the A 212-B steel is insensitive to this reagent because there is insufficient free N and C to decorate the dislocation lines. Because of this negative result, a similar study of irradiated specimens has not been undertaken.

⁸M. S. Wechsler, R. G. Berggren, N. E. Hinkle, and W. J. Stelzman, "Radiation Hardening and Embrittlement in a Low-Carbon Pressure Vessel Steel," paper presented at the Symposium on the Effects of Radiation on Structural Metals, June 26-28, 1968, San Francisco, California. To be published in the proceedings.

⁹T. R. Wilshaw and P. L. Pratt, "The Effect of Temperature and Strain Rate on the Deformation and Fracture of Mild-Steel Charpy Samples," pp. 973-991 in Proceedings First International Conference on Fracture, Vol. 2, The Japanese Society for Strength and Fracture of Materials, Japan, 1966.

The new techniques described above, along with recent improvements in older equipment, are being used to study the properties of irradiated A 212-B and A 533-B pressure-vessel steels. A major goal of these studies is to determine whether the principal effect of irradiation is to cause a change in the initiation or the propagation of cleavage fracture. The broader approach that is now available to us should make it possible to gain a deeper understanding of the effect of neutron irradiation on the phenomenon of brittle fracture.

Electron Fractography of Irradiated A 212-B Pressure-Vessel Steel
(C. R. Brooks,¹⁰ J. L. Miller, M. S. Wechsler)

The hardening and embrittlement of A 212-B pressure-vessel steel upon neutron irradiation have been reported previously.^{7,8} Tensile and impact properties were determined as a function of temperature for the unirradiated and irradiated base-plate material. These results show a radiation-induced increase in both the tensile yield stress and the DBTT of the steel as shown in Figs. 4 and 5. From the analysis of results, we concluded that the steel is embrittled because the irradiation has increased the yield strength without appreciably changing the fracture stress; that is, in the irradiated condition the steel begins to deform plastically at a higher stress level, but fracture occurs at the same stress for both conditions. Such behavior can be interpreted to mean that the irradiation has induced lattice defects that impede dislocation movement, but that the basic mechanism of the initiation and propagation of cracks is unaffected by the irradiation. If this is true, the morphology of the fracture surfaces should be identical for both conditions.

The morphology of brittle-fracture surfaces of ferritic steels is quite complex, consisting of a very fine structure of features (scale about 100 A) created by the complicated process of rapid propagation of cracks in a brittle, two-phase structure. Therefore, it is difficult

¹⁰Department of Chemical and Metallurgical Engineering, the University of Tennessee.

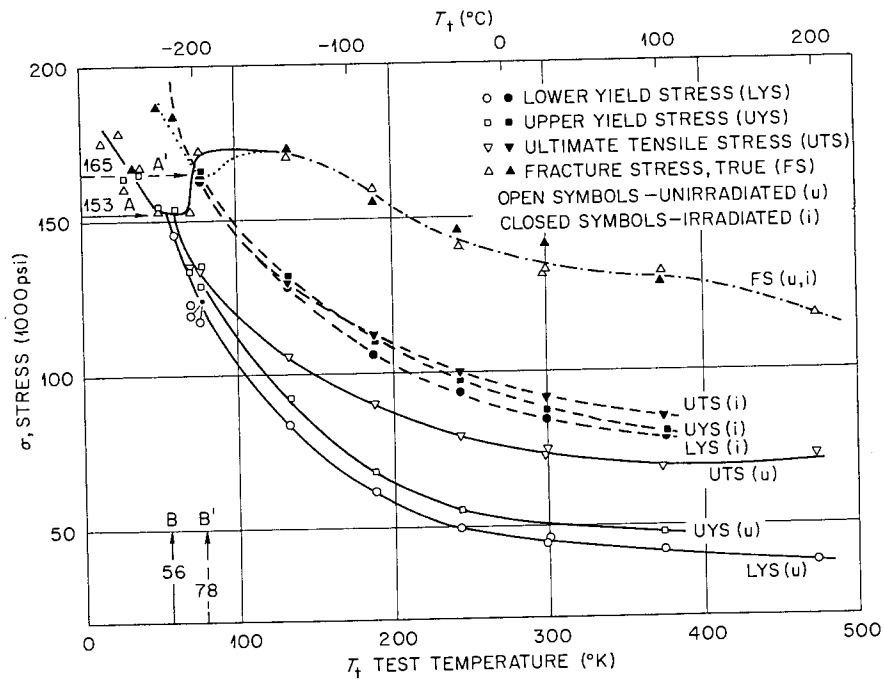


Fig. 4. Stress Versus Test Temperature for Tensile Tests on Unirradiated and Irradiated A 212-B Steel. Fluence, 1.0×10^{19} neutrons/cm², (> 1 Mev). Irradiation temperature, 60°C. Strain rate, 2.7×10^{-4} sec⁻¹. Ref.: M. S. Wechsler, R. G. Berggren, N. E. Hinkle, and W. J. Stelzman, "Radiation Hardening and Embrittlement in a Low-Carbon Pressure Vessel Steel," paper presented at the Symposium on the Effects of Radiation on Structural Metals, June 26-28, 1968, San Francisco, California. To be published in the proceedings.

to determine the sequence of events taking place as the steel fractures or to draw conclusions concerning the mechanism of initiation and growth of cracks. However, it is useful to characterize certain morphological features common on brittle-fracture surfaces, such as river patterns (see Ref. 11), as a function of the variables of heat treatment and irradiation.

Details of the fine structure of fracture surfaces can be obtained by electron fractography. This involves replicating the surface with plastic tape, coating the replica with C, shadowing with a metal such as Pt to improve contrast, and then dissolving the plastic. The secondary replica is thin enough to transmit electrons in the electron

¹¹Electron Fractography, Am. Soc. Testing Mater. Spec. Tech. Publ. 436, American Society for Testing and Materials, Philadelphia, Pennsylvania, 1967.

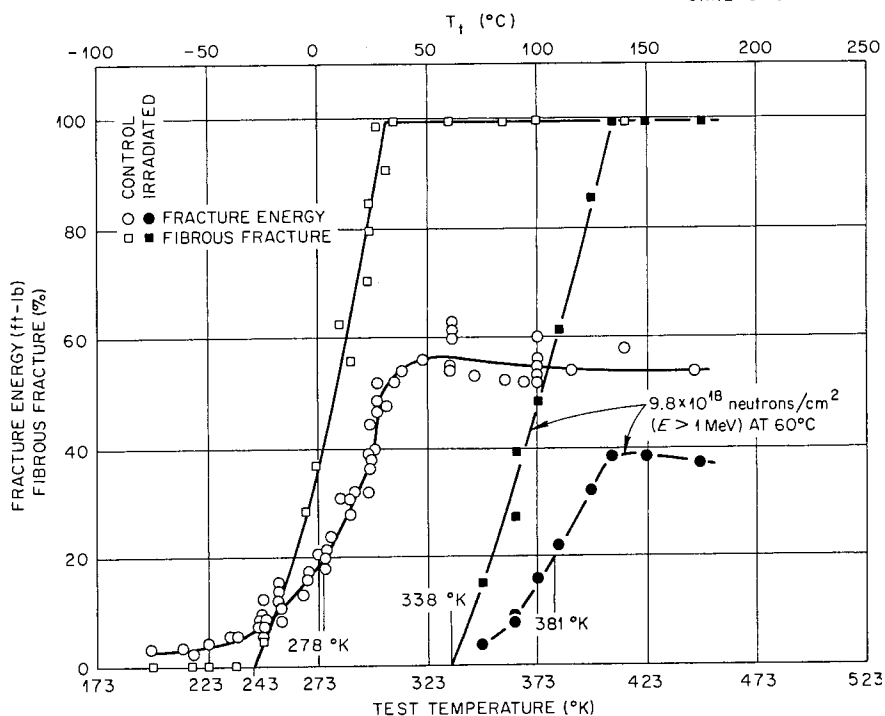


Fig. 5. Fracture Energy and Fibrous Fracture Appearance Versus Test Temperature for Impact Tests on Unirradiated and Irradiated A 212-B Steel. Ref., M. S. Wechsler, R. G. Berggren, N. E. Hinkle, and W. J. Stelzman, "Radiation Hardening and Embrittlement in a Low-Carbon Pressure Vessel Steel," paper presented at the Symposium on the Effects of Radiation on Structural Metals, June 26-28, 1968, San Francisco, California. To be published in the proceedings.

microscope, and an image of the surface that has good contrast is generated. The resolution of the image is limited by the plastic replica itself to about 100 Å; the depth of field of the electron microscope allows the uneven surface to remain in focus. Thus, by electron fractography, we observe a replica of the fracture surface that reveals the fine details of the surface morphology.

We observed specimens from two heats of ASTM A 212-B steel, for which chemical analyses and heat treatments are given in Table 1. The heat treatments produced a soft steel with a microstructure of free ferrite and regions of rather coarse pearlite. Optical and electron micrographs of the microstructure of the unirradiated base plate are shown in Fig. 6. A comparison of microstructures for the unirradiated and irradiated steel is shown in the electron micrographs of Fig. 7;

Table 1. ASTM A 212-B Pressure-Vessel Steel^a

Heat	Chemical Composition, wt %				
	C	Mn	Ph	S	Si
Item 157	0.36	0.62	0.012	0.033	0.18
Item 147	0.25	0.74	0.013	0.025	0.20

^aHeat treatment: 2 3/4-in.-thick plate was normalized at about 900°C, cooled by water spray to 260°C, and stress relieved at 650 to 680°C; all specimens for impact and tensile tests were taken from quarter thickness.

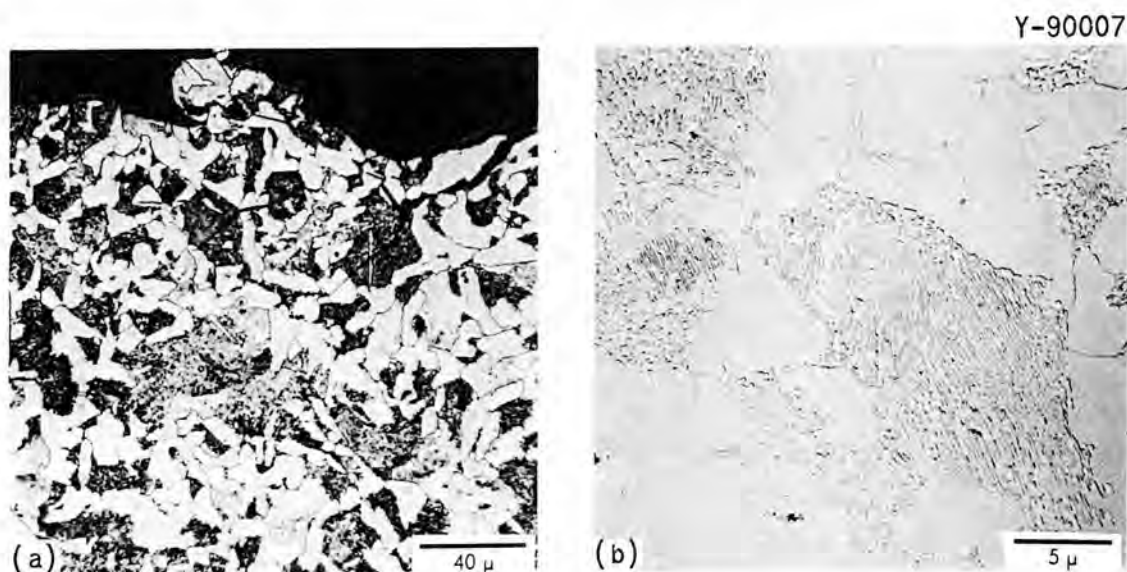


Fig. 6. Microstructure of Unirradiated ASTM A 212-B Pressure-Vessel Steel. (a) Optical micrograph showing edge of fracture surface of Charpy V-notch specimen. (b) Electron micrograph of replica of etched microstructure.

these were obtained by replicating polished and etched longitudinal sections near the fracture surfaces of tensile samples tested at low temperatures. No gross features distinguish the irradiated microstructure from the unirradiated one, except possibly for slight difference in the etching behavior that give rise to small pockmarks within ferrite grains in the irradiated steel.

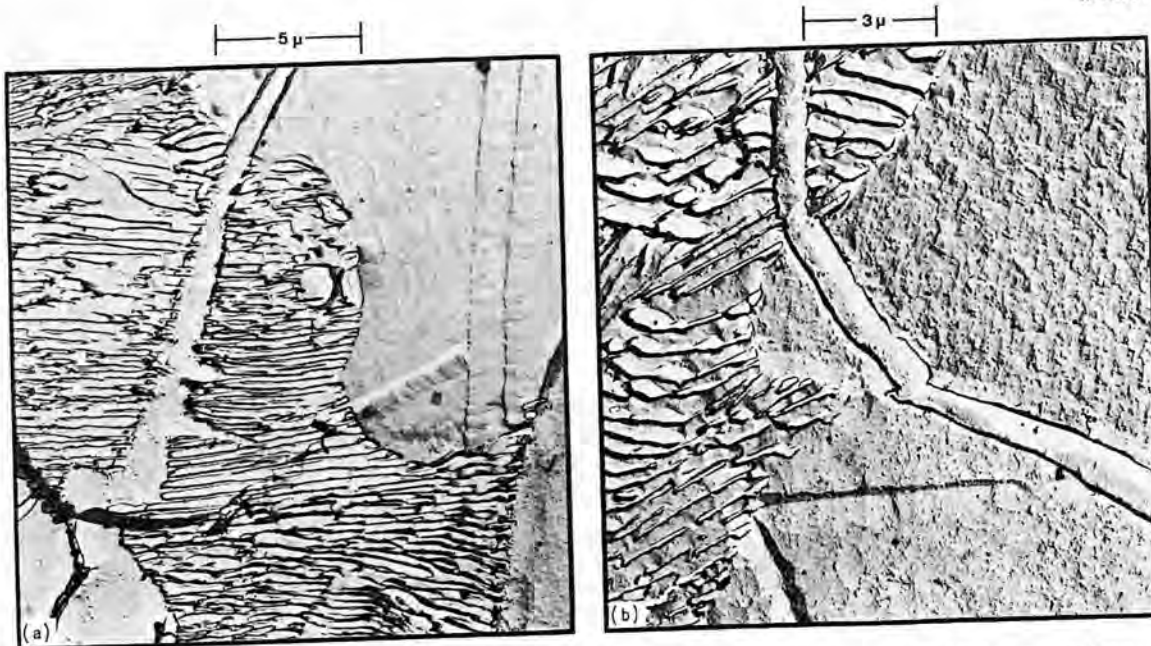


Fig. 7. Electron Micrographs of a Polished and Etched Section near the Fracture of Unirradiated and Irradiated Tensile Specimens of A 212-B Steel. (a) Unirradiated, $T_t = 50$ K. (b) Irradiated, $T_t = 34$ K, $\Phi = 1.0 \times 10^{19}$ neutrons/cm² at 60°C.

Electron fractographs were obtained on tensile and impact specimens irradiated near 60°C to a fluence of 1×10^{19} neutrons/cm² (> 1 Mev). The irradiation produced an increase in DBTT of 95°C (Fig. 5). The fractographs of the unirradiated tensile specimen tested at 77 K (-196°C) and the irradiated tensile specimen tested at 34 K (-239°C) are shown in Fig. 8; both specimens fractured brittly (i.e., before a lower yield stress was reached). The pearlite platelets are clearly revealed in both cases, and no obvious differences are apparent in the morphologies of the unirradiated and irradiated fracture surfaces. Electron fractographs for impact specimens from Item 147 (Table 1) are shown in Figs. 9 and 10. The irradiations in this case were carried to 8×10^{18} neutrons/cm² (> 1 Mev) at 340°C, and despite the high irradiation temperature, the DBTT was increased about 30°C. All specimens were tested at temperatures below the DBTT. Figure 9 compares the unetched fracture surfaces of unirradiated and irradiated specimens; the fracture surfaces look quite similar. Figure 10 shows the surfaces in the etched condition. The microstructure is more clearly revealed in this

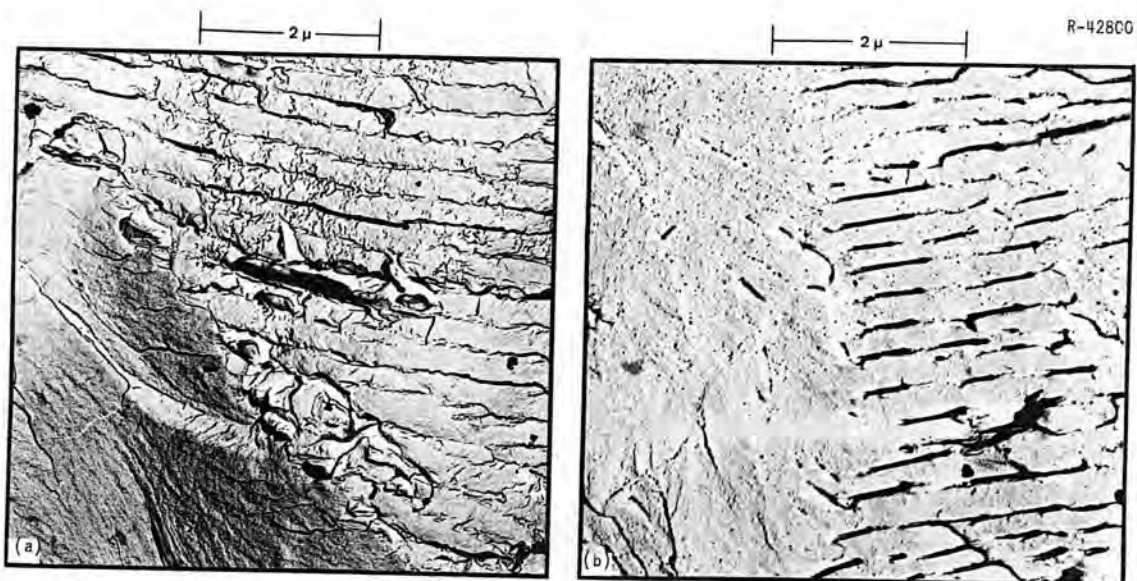


Fig. 8. Electron Fractographs of Unirradiated and Irradiated Tensile Specimens of A 212-B Steel. (a) Unirradiated, $T_t = 77$ K. (b) Irradiated, $T_t = 34$ K. $\Phi = 1.0 \times 10^{19}$ neutrons/cm² at 60°C.

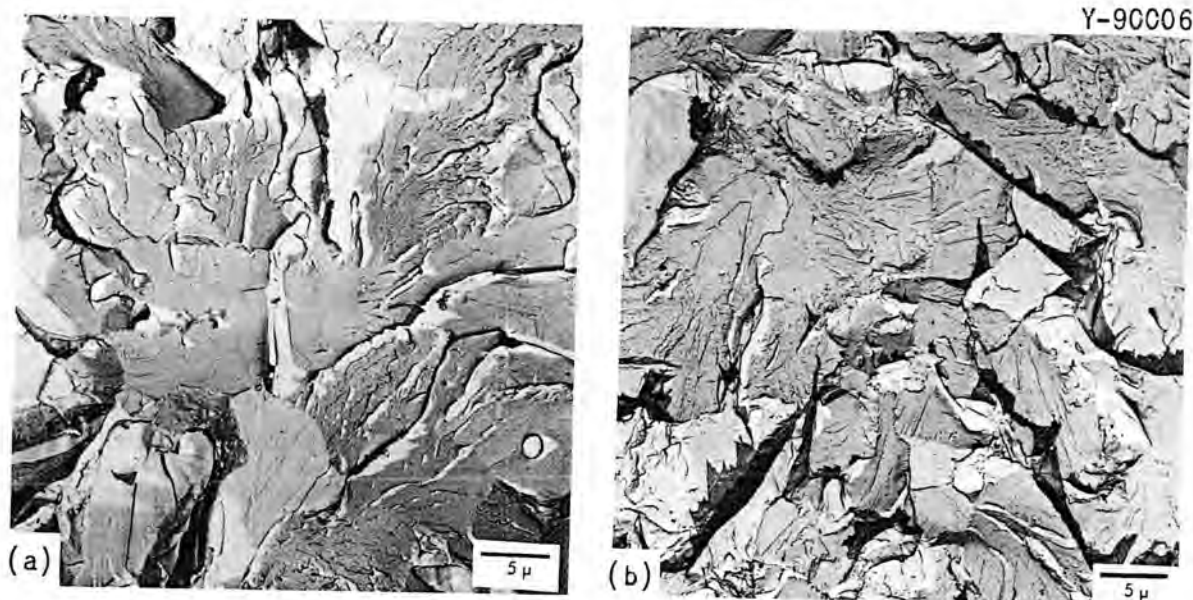


Fig. 9. Electron Micrographs of Replicas of Unetched Fracture Surface of Charpy V-Notch Impact Specimens of Unirradiated and Irradiated A 212-B Steel (Item 147). (a) Unirradiated, fractured at -60°C , 3 ft-lb. (b) Irradiated, 8.3×10^{18} neutrons/cm² at 340°C for 45 days, fractured at -40°C , 2 ft-lb.

Y-90069

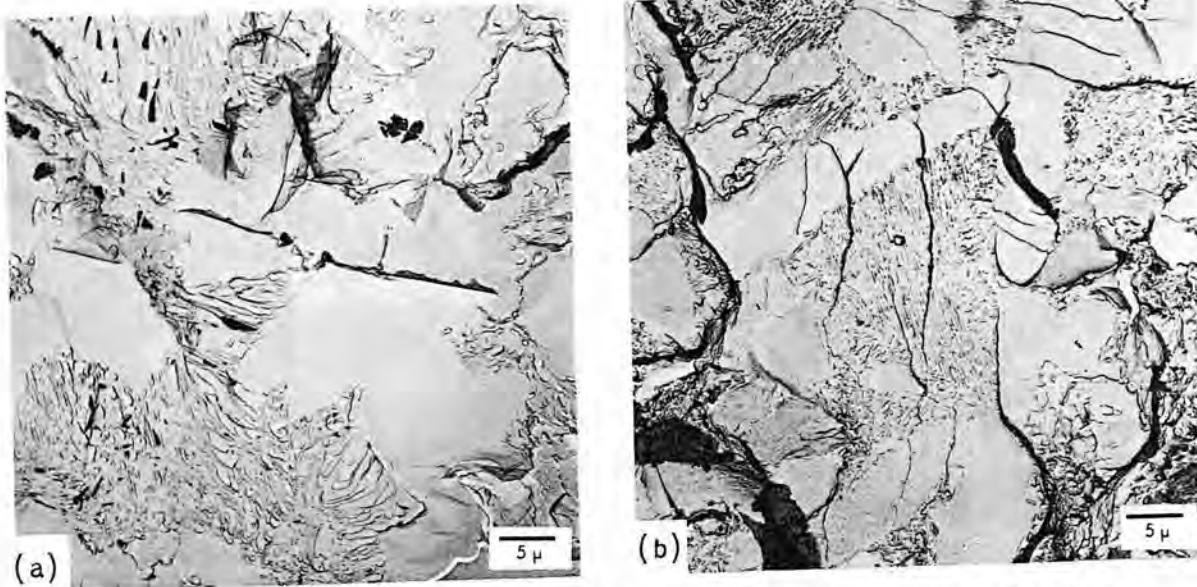


Fig. 10. Electron Micrographs of Replicas of Etched Fracture Surface of Charpy V-Notch Impact Specimens of Unirradiated and Irradiated A 212-B Steel (Item 147). (a) Unirradiated, fractured at -60°C , 3 ft-lb. (b) Irradiated, 8.3×10^{18} neutrons/cm² at 340°C for 45 days, fractured at -40°C , 2 ft-lb. Etched.

case, but again no gross difference is visible in the fracture morphology upon irradiation.

Transmission electron microscopy is another technique we have applied to the irradiated pressure-vessel steels. Figure 11 shows electron transmission micrographs for unirradiated and irradiated [8×10^{18} neutrons/cm², (> 1 Mev) at 70°C] foils from Item 147 (Table 1) taken with a Hitachi 200 kev electron microscope. The foils were deformed about 5% by rolling before chemical thinning. The micrograph (Fig. 11) for the irradiated foil does not indicate any defect clusters or spot contrast, as has been observed for many other irradiated metals. In a similar attempt, Birkle and Rall¹² were also unable to observe defect clusters produced by irradiation of A 212-B steel. Some differences in the dislocation configurations for the unirradiated and irradiated foils are apparent, however, in Fig. 11. The dislocations

¹²A. J. Birkle and W. Rall, Trans. Met. Soc. AIME 230, 156-163 (1964).

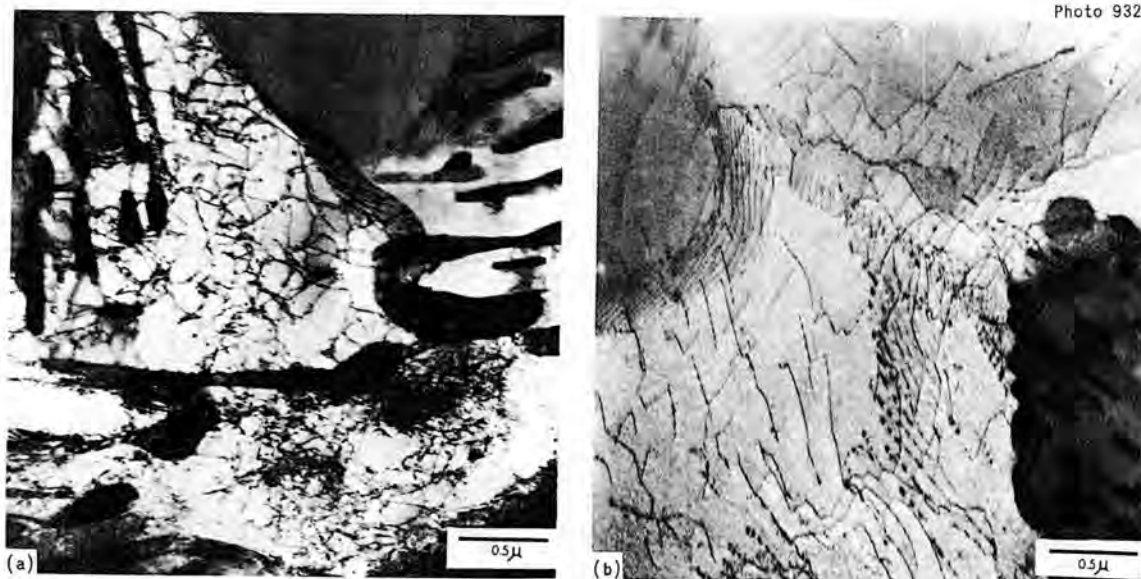


Fig. 11. Transmission Electron Micrographs of Unirradiated and Irradiated A 212-B Steel Strained about 5%. (a) Unirradiated. (b) Irradiated, 8×10^{18} neutrons/cm², 70°C.

generated by the rolling treatment appear somewhat clustered and tangled for the unirradiated foil, whereas for the irradiated one they lie in long strands along crystallographic directions. This is probably due to a type of dislocation channeling, such as that observed by Mastel *et al.*¹³ for Mo or Tucker *et al.*¹⁴ for Nb, but the absence of visible defect clusters in the transmission electron micrographs makes a study of the phenomenon considerably more difficult in ferritic steels.

Radiation Hardening and Embrittlement in ASTM A 533-B Steel
(R. G. Berggren, W. J. Stelznan, T. N. Jones, M. S. Wechsler)

Specimens for tensile and Charpy V-notch impact tests were taken from the surface, quarter-thickness, and midthickness locations of HSST (Heavy Section Steel Technology) Plate 01, a 12-in.-thick ASTM A 533-B Class 1 manganese-molybdenum-nickel steel plate. All specimens were of longitudinal orientation; that is, the tension axis of each specimen

¹³B. Mastel, H. E. Kissinger, J. A. Laidler, and T. K. Bierlein, *J. Appl. Phys.* 34, 3637-3638 (1963).

¹⁴R. P. Tucker, M. S. Wechsler, and S. M. Ohr, "Dislocation Channeling in Neutron-Irradiated Niobium," to be published in *Journal of Applied Physics*.

Table 2. Tensile Properties of Irradiated 12-in.-Thick A 533-B Steel^a from Heat A-1008-1, HSST Plate 01

Specimen Number	Fluence [neutrons/cm ² (> 1 Mev)]	Irradiation Temperature (°C)	Strength Properties, psi			Elongation, %	
			Upper Yield	Lower Yield	Ultimate ^b Tensile	Uniform	Total ^c
	× 10 ¹⁸		× 10 ³	× 10 ³	× 10 ³		
Quarter-Thickness Specimens							
6000			70.7	68.5	90.2	8.9	17.6
6001			69.9	69.1	90.8	10.0	18.3
6036			69.8	68.6	90.3	10.0	18.8
6037			69.4	68.6	89.7	9.6	19.2
6054			69.7	68.1	89.2	10.7	22.1
6055			69.2	67.9	89.8	9.5	19.4
6064			69.1	67.5	89.2	10.2	21.4
6065			68.4	67.8	89.3	9.6	18.9
Average			69.5	68.3	89.8	9.8	19.5
6061	7.2	63	104.0	101.1	102.2	5.2	13.6
6033	7.7	65	107.0	102.4	103.6	4.2	13.0
6060	8.6	232	94.8	92.8	107.7	9.0	16.2
6032	8.9	232	96.1	94.7	108.8	8.7	15.5
6034	11.8	288	90.2	87.6	106.5	9.5	16.8
Midthickness Specimens							
6077			69.6	68.2	90.1	9.4	18.0
6078			69.1	68.1	89.9	9.6	18.0
6112				68.1	89.8	8.3	17.4
6113			68.2	67.8	90.1	9.9	18.8
Average			69.0	68.0	90.0	9.3	18.0
6086	6.9	65	106.6	102.4	103.2	4.5	12.3
6092	7.6	65	108.4	104.2	105.3	4.9	11.8
6079	7.7	232	95.2	94.6	108.9	7.8	14.5
6085	8.8	232	96.6	95.9	110.7	7.5	14.1
6093	10.3	288	87.8	86.7	106.5	9.1	15.8
6099	11.6	288	88.5	86.1	105.6	7.8	14.7

^aAll specimens are of longitudinal orientation, tested at 27°C.

^bUltimate tensile strength is here defined as the maximum load after the yield point divided by original area of cross section.

^cLength-to-diameter ratio: 7.

was parallel to the rolling direction. These specimens were irradiated to fast-neutron fluences of 5 to 11×10^{18} neutrons/cm² (> 1 Mev) at temperatures of 66, 232, 288, and 343°C.

Results of tensile tests on specimens from quarter-thickness and midthickness, irradiated at 66, 232, and 288°C and tested at room temperature, are presented in Table 2. Results from impact tests of Charpy V-notch quarter-thickness specimens, irradiated at 68, 232, and 293°C, are presented in Fig. 12.

The purpose of these tensile and impact tests was to determine the effect of varying the irradiation temperature over the range cited above. However, because of flux variations in the irradiation capsules and differences in core loading from one experiment to the other, it was necessary to accept the differences in fluences noted in Table 2 and Fig. 12. To correct for the differences in fluence, we assumed that the increase in yield stress and the increase in DBTT are proportional to the square root of the fluence. On this basis, the increase in yield stress upon irradiation at 232 and 288°C are about 74 and 42%, respectively, of the increase in yield stress for the 68°C irradiation. The effect of irradiation temperature, analyzed in this way, was about the same for quarter-thickness and midthickness specimens, although the increases in yield stress normalized to a given fluence were slightly greater for midthickness specimens.

For impact results (Fig. 12) it is difficult to make a similar comparison because the impact curves are not parallel and because the comparison would depend on the fracture energy at which the transition temperature were fixed. It turns out that for a 25 ft-lb criterion the increases in DBTT upon irradiation at 232 and 288°C are about 87 and 43%, respectively, of the increase in DBTT for the 68°C irradiation. These percentages are roughly in agreement with those for the tensile tests, but the agreement is somewhat fortuitous for the reason mentioned above.

It was stated earlier in this report¹⁵ that the cleavage fracture stress under impact conditions may be determined by the intersection of

¹⁵N. E. Hinkle et al., "Radiation Hardening and Embrittlement in ASTM A 212-B Steel," pp. 174-182, this report.

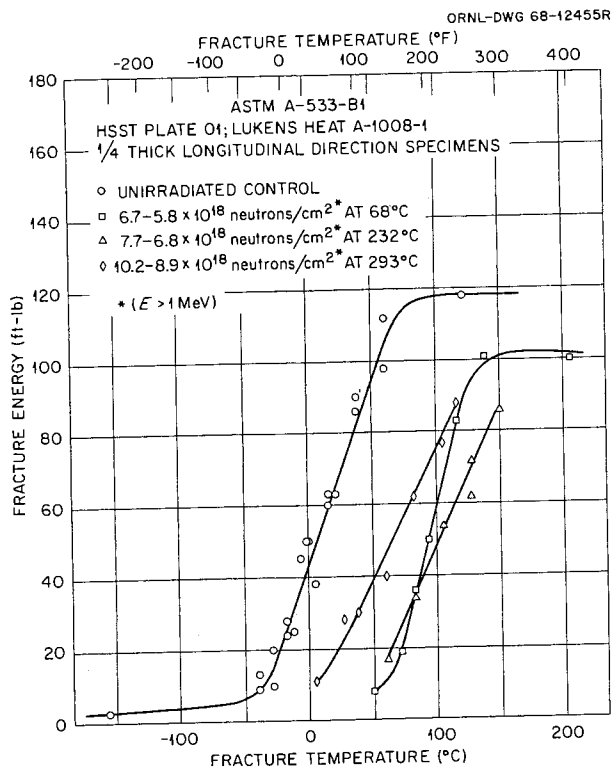


Fig. 12. Effect of Neutron Irradiation at Three Temperatures on the Notch-Impact Properties of Quarter-Thickness Specimens from a 12-in.-Thick Plate of Manganese-Molybdenum-Nickel Steel (ASTM A 533-B Class 1, HSST Plate 01).

general yield load and maximum (or fracture) load curves. Furthermore, one criterion for the DBTT is that temperature at which the yield stress reaches the cleavage-fracture stress. Hence, the DBTT is given by the temperature where the curves for general yield load and maximum load intersect. To determine this DBTT, oscilloscope records of load versus time during impact were obtained for most of the impact tests presented above. General yield loads and maximum loads obtained from these records are presented in Fig. 13. Zero-ductility transition temperatures may be determined by extrapolating to zero energy the steep portion of the curves for fracture energy in Fig. 12. These transition temperatures may be compared with those obtained from the intersection of the plots of the maximum load and general yield load recorded by the oscilloscope during notch-impact testing. Such results are given in Table 3. The data now available show that the transition temperatures

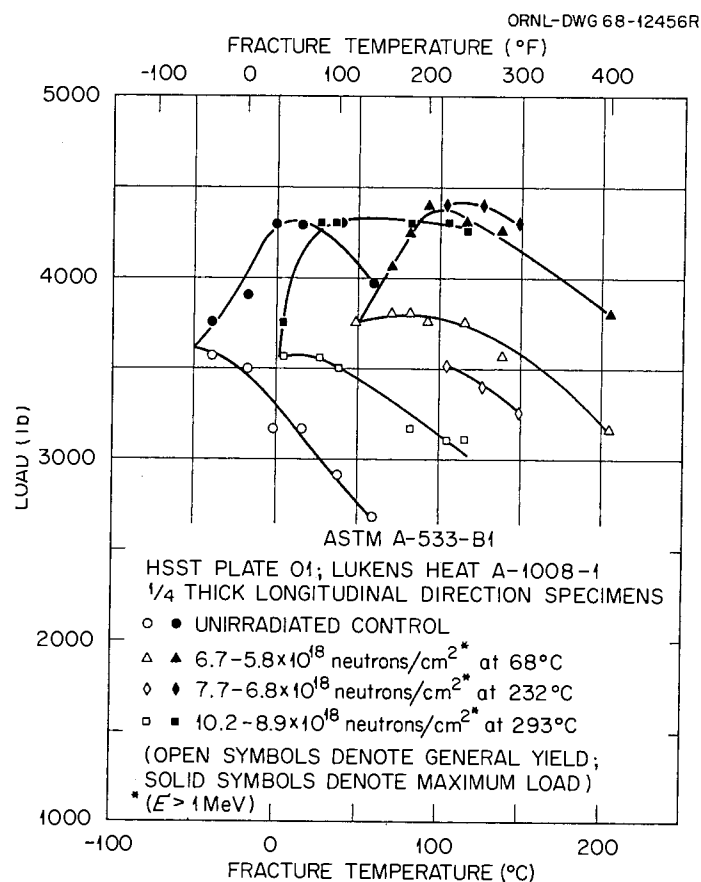


Fig. 13. General Yield and Maximum Loads During Notch-Impact Testing of Quarter-Thickness Specimens from a 12-in.-Thick Plate of Manganese-Molybdenum-Nickel Steel (ASTM A 533-B Class 1, HSST Plate 01).

Table 3. Comparison of Transition Temperatures of Irradiated ASTM A 533-B Class 1 Steel (Quarter-Thickness Charpy V-Notch Impact Specimens from HSST Plate 01)

Specimen Condition	Temperature, °C	
	At Zero Fracture Energy Intercept	Intersection of General Yield Load and Maximum Load Curves
Unirradiated	-44	-51
Irradiated to 6 × 10 ¹⁸ neutrons/cm ² (> 1 Mev) at 68°C	58	49
Irradiated to 1 × 10 ¹⁹ neutrons/cm ² at 293°C	-1	4

obtained by these two methods agree within the probable accuracy of the analysis. The present results indicate that the relationship between radiation hardening and embrittlement developed^{16,17} for a different steel (ASTM A 212-B) will probably also apply to this ASTM A 533-B Class 1 steel.

Properties of 12-in.-Thick ASTM A 533-B Class 1 and Class 2 Steels
(R. G. Berggren, T. N. Jones)

Characterization tests continue on unirradiated 12-in.-thick plates of ASTM A 533-B (Manganese-Molybdenum-Nickel Steel Plate, Quenched and Tempered for Pressure Vessels). A portion of this material is included in several studies of radiation effects.

The first three plates (HSST plates 01, 02, and 03) were produced by Lukens Steel Company and heat treated to Class 1 specifications: The first two were heat treated by Combustion Engineering, Inc., and the third was heat treated by Lukens Steel Company. The HSST plates 01 and 02 were heat treated as identically as possible: both plates were dip quenched, edge down, in agitated water. The HSST plate 03 was flat quenched in agitated water so that possible effects of steam binding during quenching could be determined.

Test results for the central region of HSST plate 01 have been reported previously,^{18,19} and those for the central region of HSST plate 02 have now been obtained. Tensile test results (ASTM standard 0.505-in.-diam specimens) for HSST plate 02 are presented in Table 4.

¹⁶M. S. Wechsler, N. E. Hinkle, R. G. Berggren, and W. J. Stelzman, Radiation Metallurgy Section Solid State Division Progress Report for Period Ending January 1968, ORNL-4246, pp. 6-27.

¹⁷M. S. Wechsler, R. G. Berggren, N. E. Hinkle, and W. J. Stelzman, "Radiation Hardening and Embrittlement in a Low-Carbon Pressure Vessel Steel," paper presented at the Symposium on the Effects of Radiation on Structural Metals, June 26-28, 1968, San Francisco, California. To be published in the proceedings.

¹⁸R. G. Berggren and T. N. Jones, Radiation Metallurgy Section Solid State Division Progress Report for Period Ending January 1968, ORNL-4246, pp. 38-41.

¹⁹F. J. Witt, Heavy Section Steel Technology Program Semiann. Progr. Rept. Feb. 29, 1968, ORNL-4315, pp. 19-28.

Table 4. Tensile Properties of 12-in.-Thick A 533-B
Class 1 Steel from Heat 1195-1, HSST Plate 02

Specimen Number	Test Temper- ature (°C)	Strength Properties, psi				Percent	
		Upper Yield	Lower Yield	Ultimate Tensile	True Fracture	Total Elongation	Reduction in Area
		$\times 10^3$	$\times 10^3$	$\times 10^3$	$\times 10^3$		
Top-Surface Specimens - Longitudinal ^a							
6440	24	85.8	80.9	96.95	199.1	29.0	69.9
6441	24	85.8	81.0	96.95	197.9	29.2	69.5
6442	232	71.8	70.9	91.2	189.9	23.8	67.9
6443	232	71.3	70.3	92.25	189.4	23.8	66.8
6444	288		70.9 ^b	96.55	168.8	23.8	58.6
6445	288		70.8 ^b	96.3	174.5	23.8	61.1
6446	343		68.4 ^b	91.75	172.6	25.0	65.9
6447	343		67.9 ^b	91.35	163.7	28.0	64.0
Quarter-Thickness Specimens - Longitudinal ^a							
6448	24	72.3	69.9	91.05	180.6	26.0	67.9
6449	24	72.1	69.85	91.15	174.4	26.0	65.6
6450	232	61.4	61.0	86.4	180.4	25.0	66.8
6451	232	61.5	61.2	86.2	178.9	23.4	66.8
6452	288		61.9 ^b	89.85	166.4	23.5	61.6
6453	288		62.4 ^b	89.8	144.4	23.5	55.7
6454	343		60.4 ^b	87.6	157.4	27.6	62.6
6455	343		60.9 ^b	87.3	156.0	27.0	61.6
Midthickness Specimens - Longitudinal ^a							
6456	24	68.3	67.9	89.15	76.5	23.5	51.7
6457	24	69.55	68.6	89.4	152.5	25.2	56.8
6458	232	60.2	59.9	84.8	136.4	22.2	51.7
6459	288		62.4 ^b	88.85	139.9	21.2	48.6
6460	288		61.4 ^b	87.7	135.5	21.0	48.0
6461	343		59.9 ^b	85.8	107.1	23.5	41.3
Top-Surface Specimens - Transverse ^c							
6467	24	87.5	80.4	97.1	194.1	28.4	63.0
6468	24	86.9	80.9	97.05	191.2	28.4	66.6
6472	288		70.9 ^b	96.45	161.8	23.8	58.3
6475	288		70.7 ^b	95.9	133.6	19.2	40.7

Table 4 (continued)

Specimen Number	Test Temperature (°C)	Strength Properties, psi				Percent	
		Upper Yield	Lower Yield	Ultimate Tensile	True Fracture	Total Elongation	Reduction in Area
		$\times 10^3$	$\times 10^3$	$\times 10^3$	$\times 10^3$		
Quarter-Thickness Specimens - Transverse ^c							
6464	24	71.85	69.1	91.0	170.2	26.5	63.0
6465	24	71.4	69.2 _b	91.35	160.7	24.6	60.8
6473	288		62.4 _b	89.9	131.9	19.2	42.5
6476	288		62.4 _b	90.4	159.6	23.0	56.5
Midthickness Specimens - Transverse ^c							
6466	24	68.75	67.75	88.5	65.6	13.6	25.8
6469	24		70.2 _b	91.3	64.3	19.8	38.1
6474	288		62.4 _b	87.7	130.5	19.8	43.4
6477	288		61.9 _b	84.2	73.9	9.2	21.6
Quarter-Thickness Specimens - Perpendicular ^d							
6470	24	71.1	69.0	91.05	136.7	23.8	57.3
6478	24	70.4	69.0 _b	91.0	136.6	23.2	50.5
6471	288		62.9 _b	88.9	139.9	19.0	45.7
6479	288		63.15 _b	89.65	152.1	21.0	51.6

^a Longitudinal specimen: tension axis parallel to rolling direction.

^b Lower yield stress reported is 0.2% offset yield strength.

^c Transverse specimen: tension axis transverse to the rolling direction and in the rolling plane.

^d Perpendicular specimen: tension axis perpendicular to the rolling plane (plate surface).

The yield and ultimate strengths were found to be insensitive to specimen orientation. True fracture stress, elongation, and reduction of area were dependent on specimen orientation, the greatest orientation effect being at the half-thickness level due to the higher concentration of inclusions in the center of the plate thickness.

Charpy V-notch impact tests were conducted on HSST plate 02; the results are shown in Table 5 and Figs. 14 and 15. The major effect of specimen orientation was to lower fracture energies in the ductile portion of the energy-temperature curve (ductile shelf) for the transverse and perpendicular orientations. This is shown in Table 5 and Fig. 14. As observed for HSST plate 01, the energy-temperature curves for quarter-thickness and midthickness specimens were identical (Fig. 15), and a lower transition temperature was observed for surface specimens. The lower transition temperature of surface specimens is a result of the higher cooling rates near the surface of the plate during quenching.

Table 5. Drop Weight and Charpy-V Impact Properties of 12-in.-Thick ASTM A 533-B Class 1 Steel from Heat No. 1105-1, HSST Plate 02

Level in Plate	Orientation ^a	Temperature, °C		Energy, ft-lb	
		Drop-Weight Nil-Ductility ^b	Charpy-V Transition ^c	Ductile Shelf	Nil-Ductility Transition Correlation
Surface	L		-84	105	50
	T	-68	-73	85	35
Quarter-thickness	L		-7	115	25
	T	-15	-1	95	25
	P		10	80	18
Half-thickness	L		-7	95	25
	T	-12	16	90	15

^aL: long axis of specimen longitudinal (parallel to plate surface).
 T: Long axis of specimen transverse to rolling direction and parallel to plate surface.
 P: long axis of specimen perpendicular to plate surface.

^bP-3 drop-weight specimens.

^cTransition temperature for 32 ft-lb fracture energy.

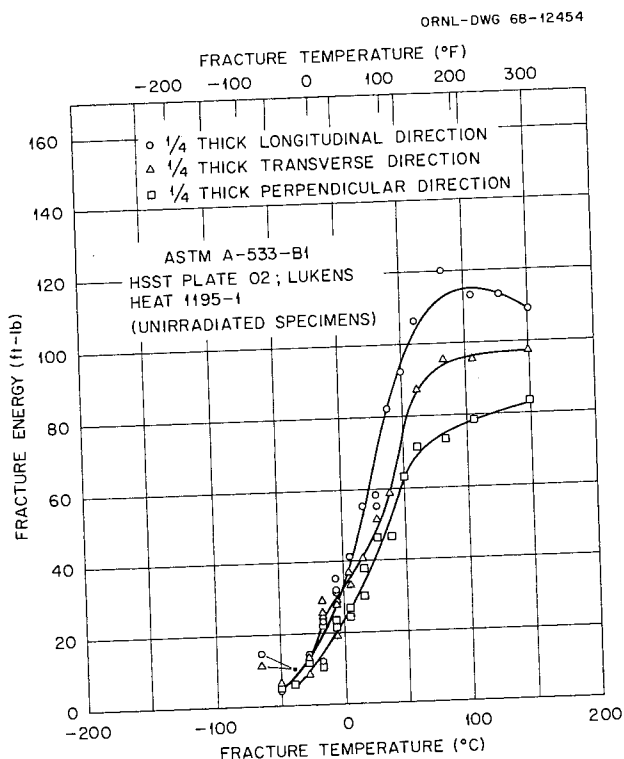


Fig. 14. Charpy V-Notch Impact Test Results for Three Specimen Orientations at the Quarter-Thickness Level in a 12-in.-Thick Plate of Manganese-Molybdenum-Nickel Steel (ASTM A 533-B Class 1, HSST Plate 02).

Drop-weight tests were also performed on surface, quarter-thickness, and midthickness specimens of transverse orientation. These results are given in Table 5. The effect of depth in plate agreed with the results from the Charpy tests: the surface specimens had a lower nil-ductility transition (NDT) temperature than quarter-thickness or midthickness specimens, and quarter-thickness and midthickness specimens had essentially the same NDT.

Several mechanical properties of HSST plates 01 and 02 are compared in Fig. 16 (properties of HSST plate 04, included in this figure, are discussed separately). These results show that the mechanical properties of HSST plates 01 and 02 are almost identical. Both plates meet the ASTM specifications and are uniform in properties through the central 8 in. with the exception of lower ductilities in the central 1 in. Material from these plates is satisfactory for studies of radiation effects. Material from HSST plate 01 is being used in one series of studies of radiation effects, and the results from this series should

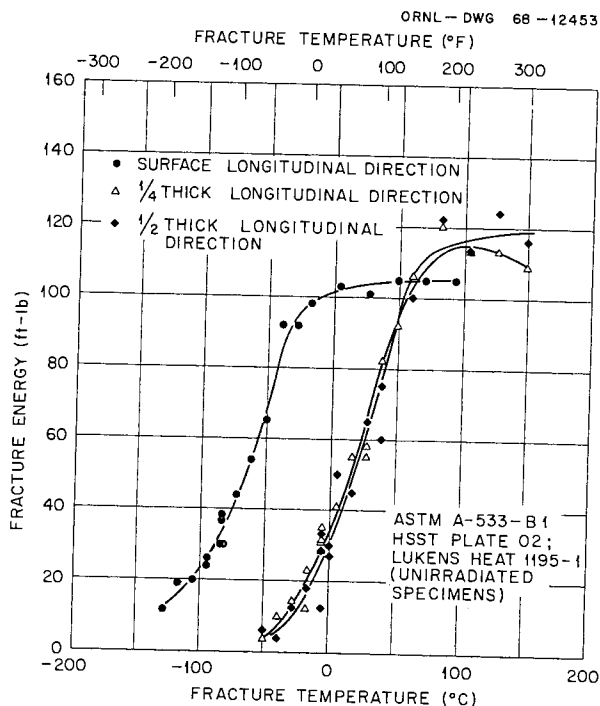


Fig. 15. Charpy V-Notch Impact Test Results for Specimens from Three Depth Levels in a 12-in.-Thick Plate of Manganese-Molybdenum-Nickel Steel (ASTM A 533-B Class 1, HSST Plate 02).

be comparable to results from studies using HSST plate 02 material, since the two plates are almost identical in unirradiated properties.

Test specimens are now being machined from HSST plate 03 (which was flat quenched).

The fourth 12-in.-thick A 533 plate (HSST plate 04) produced by Lukens Steel Company for the HSST program was cut into several sections, and parts were rerolled to 4- and 8-in. thicknesses. Segments of 4-, 8-, and 12-in. thickness were then heat treated by Lukens to ASTM A 533-B Class 2 properties. Mechanical testing by Lukens showed that the ASTM specifications could be attained but that ASME Section III toughness requirements could only be met in the 4- and 8-in.-thick plates. These segments of HSST plate 04 were flat quenched. One segment of the 12-in.-thick plate was retained in the mill-annealed condition for study of heat-treatment parameters.

We have obtained preliminary results of tensile and notch-impact tests for material near a corner (one plate thickness from edges) of

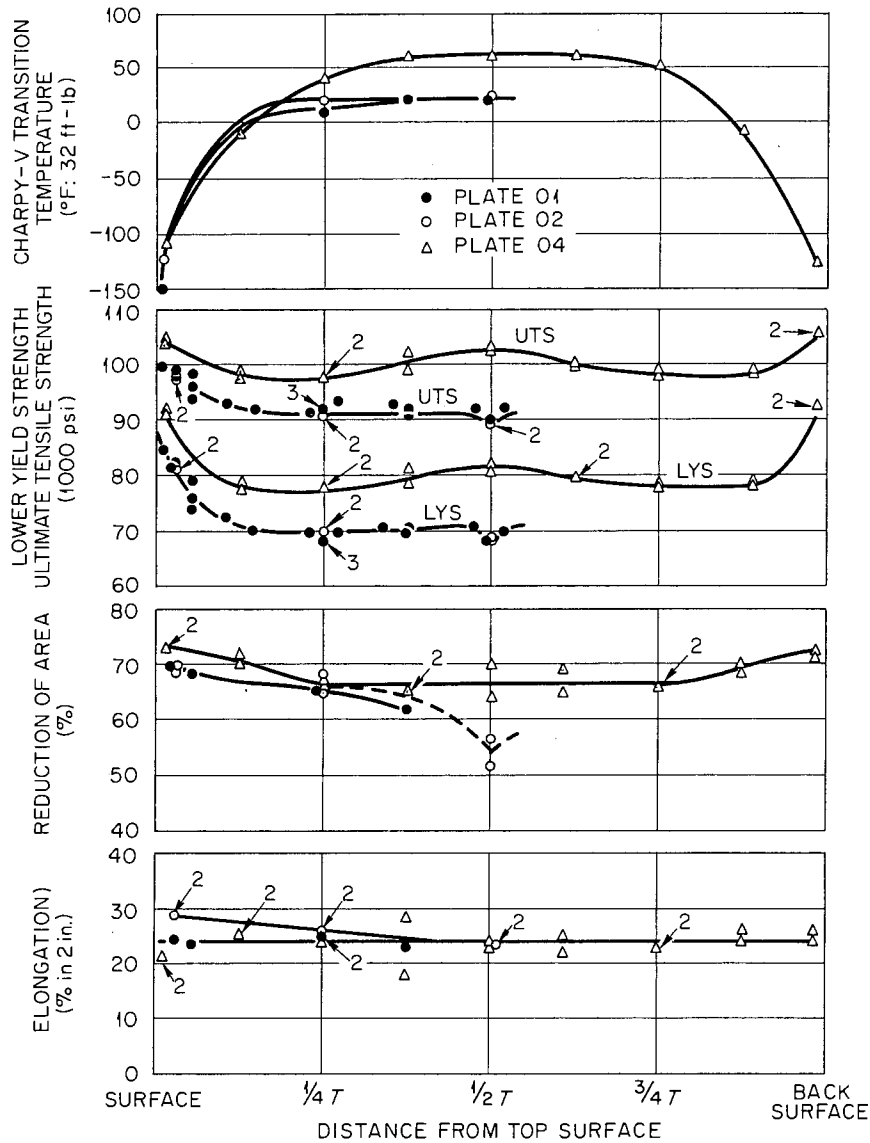


Fig. 16. Comparison of Mechanical Properties of Several Levels in Three 12-in.-Thick Plates of Manganese-Molybdenum-Nickel Steel (ASTM A 533-B Classes 1 and 2, HSST Plates O1, O2, and O4).

Table 6. Tensile Properties of 12-in.-Thick A 533-B Class 2 Steel^a from Heat C-2748-2, HSST Plate 04

Specimen Number	Strength Properties, psi				Total Elongation ^b (%)	Reduction in Area (%)
	Upper Yield	Lower Yield	Ultimate Tensile	True Fracture		
	$\times 10^3$	$\times 10^3$	$\times 10^3$	$\times 10^3$		
Top-Surface Specimens						
04-2040		90.7	103.5	230.0	21.4	73
04-2041		91.6	104.1	236.0	21.6	73
One-Eighth-Thickness Specimens						
04-2042	79.0	78.4	98.7	208.0	24.9	71
04-2043	79.2	77.4	97.5	199.0	25.4	70
Quarter-Thickness Specimens						
04-2044		77.5	97.4	186.0	23.6	66
04-2045	78.4	77.6	97.2	191.0	23.9	67
Three-Eighths-Thickness Specimens						
04-2046		81.0	101.7	179.0	18.3	65
04-2047	79.3	78.3	98.6	188.0	28.4	65
Midthickness Specimens						
04-2048	82.6	81.6	102.7	230.0	24.0	70
04-2049	82.1	81.0	102.1	193.0	22.7	64
Five-Eighths-Thickness Specimens						
04-2050	80.6	79.6	100.2	216.0	21.9	69
04-2051	80.6	79.2	99.5	187.0	25.3	65
Three-Quarter-Thickness Specimens						
04-2052	78.7	78.3	98.7	186.0	23.1	66
04-2053	78.3	77.7	97.7	186.0	22.9	66
Seven-Eighths-Thickness Specimens						
04-2054	79.4	78.4	98.5	185.0	26.4	68
04-2055		77.9	97.8	202.0	23.9	70
Back-Surface Specimens						
04-2056	93.6	92.0	105.5	222.0	23.9	71
04-2057	93.4	92.0	105.3	231.0	25.9	72

^aAll specimens of longitudinal orientation (tension axis parallel to rolling direction), tested at 24°C.

^bElongation for length-to-diameter ratio (L:D) of 4; calculated from measurements for L:D ratio of 7.

the heat-treated 12-in.-thick segment of HSST plate 04. The tensile properties are presented in Table 6 and Fig. 16. Results of Charpy V-notch impact tests are also presented in Fig. 16. The mechanical properties are symmetric about the midthickness even though the plate was flat quenched.

Mill test reports, heat-treatment details, and detailed mechanical properties of HSST materials have been reported^{20,21} and will be reported in the Heavy Section Steel Technology Program Semiannual Progress Report series.

Radiation Effects in Iron

Radiation Hardening in Iron (S. M. Ohr, N. E. Hinkle, M. S. Wechsler)

Temperature Dependence. - The change in the temperature dependence of the yield stress in Fe following neutron irradiation is of considerable interest because it is a manifestation of the nature of the defects responsible for radiation hardening and because it reflects the relative importance of the defects produced by radiation as barriers to dislocation motion compared to the preirradiation barriers. We have investigated^{22,23} the temperature and strain rate dependencies of yield stress in Fe irradiated to a relatively low fluence of 1.2×10^{16} neutrons/cm² (> 1 Mev). We observed that the overall effect of neutron irradiation was an upward shift of the curve for yield stress versus test temperature without an appreciable change in its shape. We have now extended the study to a fluence of 2.7×10^{19} neutrons/cm² (> 1 Mev).

²⁰F. J. Witt, Heavy Section Steel Technology Program Semiann. Progr. Rept. Feb. 29, 1968, ORNL-4315.

²¹F. J. Witt, Heavy Section Steel Technology Program Semiann. Progr. Rept. Aug. 31, 1967, ORNL-4176.

²²S. M. Ohr and E. D. Bolling, Radiation Metallurgy Section Solid State Division Progress Report for Period Ending January 1967, ORNL-4097, pp. 13-24.

²³S. M. Ohr, R. P. Tucker, and M. S. Wechsler, "Radiation Hardening in bcc Metals Niobium and Iron," pp. 187-192 in Proceedings of the International Conference on the Strength of Metals and Alloys, Tokyo, September 4-8, 1967, Vol. 9, Supplement to the Transactions of the Japan Institute of Metals, 1968.

The starting material for this study was 1 1/4-in. bar stock of Ferrovac-E Fe (Table 7). The bar was cold rolled to 0.01-in.-thick sheet from which tensile samples of 1/2-in. gage length were punched. These samples were annealed in vacuum to achieve a uniform grain diameter of about 30 μ . The tensile samples, shielded with Cd, were irradiated at temperatures between 52 and 77°C in the poolside facility of the ORR to a fluence of 2.7×10^{19} neutrons/cm² (> 1 Mev).

Table 7. Chemical Analysis of As-Received Ferrovac-E Iron

Element	Concentration (ppm by weight)	
	Original Mill Analysis	ORNL Analysis
Fe	Base metal	Base metal
C	40	50-100
O	65	50-130
N	1	5-15
H	0.3	< 1
S	70	10
P	50	10
B		10-20
Co	70	20
Cr	100	10-30
Cu	50	20
Mo	100	10
Ni	350	400
Si	60	200
Mn	10	10
V	40	1

Figure 17 shows the dependence of the lower yield stress on the test temperature obtained in this study as well as the curves for Fe both unirradiated and neutron irradiated to 1.2×10^{16} neutrons/cm². Note that the hardening is relatively insensitive to test temperature in samples irradiated to 1.2×10^{16} neutrons/cm². However, the samples irradiated to 2.7×10^{19} neutrons/cm² show greater hardening at low test temperatures. Similar observation has been made in Nb by Wechsler *et al.*²⁴

²⁴M. S. Wechsler, R. P. Tucker, and R. Bode, "Radiation Hardening in Single Crystal Niobium - The Temperature Dependence of Yielding." To be published in Acta Metallurgica.

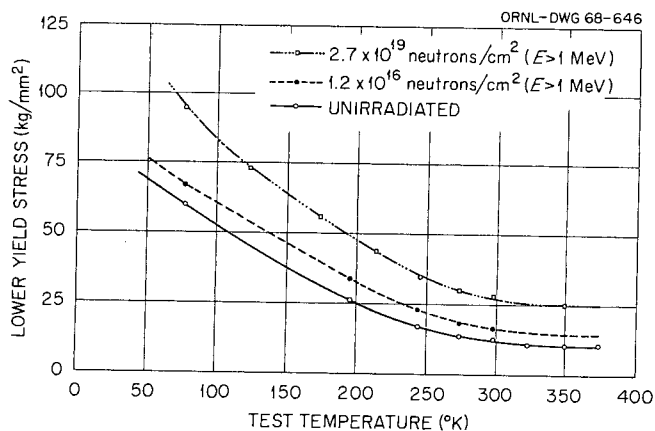


Fig. 17. The Temperature Dependence of Lower Yield Stress in Ferrovac-E Iron Unirradiated and Neutron Irradiated to Two Fluences.

They also pointed out that the hardening observed at lower test temperatures is in disagreement with a theory of radiation hardening proposed by Arsenault²⁵ which predicts a greater hardening at higher test temperatures. It is not clearly understood how an addition of new defects can give rise to a hardening that increases with decreasing test temperature. One of the difficulties associated with the problem is a lack of understanding of the nature of barriers present in Fe before irradiation.

Fluence Dependence. - It is well known that the presence of interstitial impurities can greatly influence the mechanical properties of Fe. It has also been suggested²⁶ that the irradiation hardening of Fe is sensitive to the content of interstitial impurities. Our study investigates the effect of impurity atoms (primarily interstitial C) on the dependence of radiation hardening on fluence.

The sample materials were vacuum-melted Ferrovac-E Fe with about 50 ppm C by weight, zone-refined Fe with 30 ppm C by weight, and decarburized Ferrovac-E Fe. Tensile samples with 1/2-in.-gage length were prepared from cold-rolled sheets 0.01 in. thick. Samples of zone-refined Fe, annealed in vacuum at 650°C for 20 min, gave a uniform grain size of 30 μ . Samples of Ferrovac-E Fe were similarly annealed at 750°C

²⁵R. J. Arsenault, Acta Met. 15, 1853-1859 (1967).

²⁶S. B. McRickard and J.G.Y. Chow, Acta Met. 14, 1195-2000 (1966).

for 6 hr to achieve a matching grain size of 30 μ . Samples of decarburized Fe were prepared from Ferrovac-E Fe by annealing the samples in an atmosphere of purified dry H_2 at 800°C for 72 hr. Following the decarburization treatment, the amount of C in solution as determined by measurements of internal friction was below 2 ppm, and the grain size was about 250 μ . A second group of Ferrovac-E Fe samples, annealed in vacuum at 870°C for 10 hr, resulted in a matching grain size of about 250 μ .

The samples of Fe with various interstitial impurity contents were irradiated at temperatures between 52 and 90°C in the poolside facility of the ORR at a flux of about 3×10^{12} neutrons $cm^{-2} sec^{-1}$ (> 1 Mev) to a range of fluences between 1.2×10^{16} and 2.7×10^{19} neutrons/ cm^2 (> 1 Mev).

Figure 18 shows the dependence of the lower yield stress on the square root of neutron fluence. The most noticeable feature is the rapid increase in yield stress for the Ferrovac-E Fe with a relatively high content of interstitial impurities at low neutron fluences. The rate of increase in yield stress decreases with increasing neutron fluence for all the samples studied. Note also the quick saturation of radiation hardening for Ferrovac-E Fe with the larger grain size.

It was suggested recently²⁷ that the barriers responsible for radiation hardening in Fe are complexes consisting of atoms of C and point defects produced by irradiation. Our observation is partly in agreement with such a mechanism in that rapid and greater hardening is attained in samples containing more C. It should be noted, however, that the samples of decarburized Fe also exhibit considerable hardening in the range of neutron fluences studied.

²⁷J. Diehl, G. P. Seidel, and M. Weller, "Neutron Irradiation Hardening of Iron Single Crystals Containing Small Amounts of Carbon," pp. 219-225 in Proceedings of the International Conference on the Strength of Metals and Alloys, Tokyo, September 4-8, 1967, Vol. 9, Supplement to the Transactions of the Japan Institute of Metals, 1968.

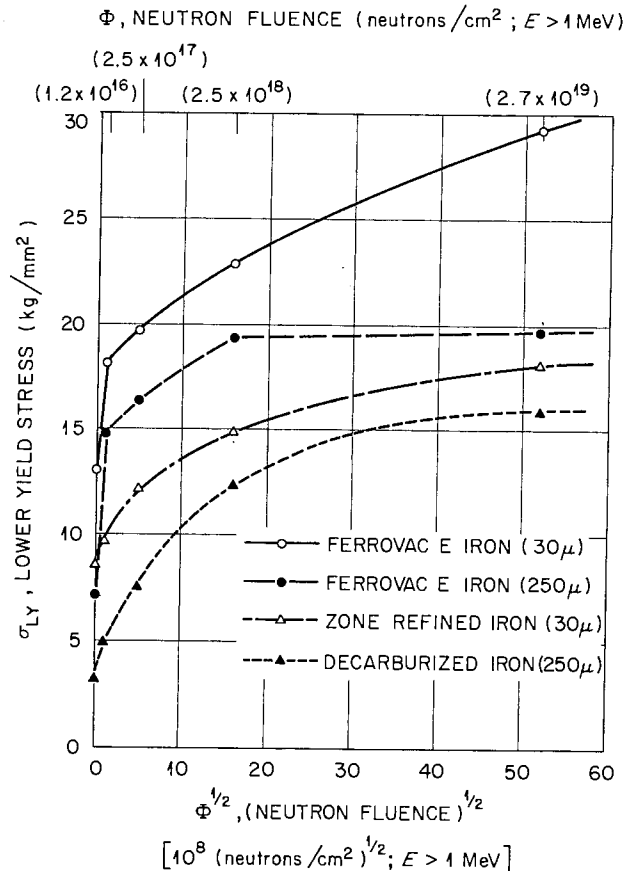


Fig. 18. The Lower Yield Stress Plotted Versus the Square Root of the Neutron Fluence for Ferrovac-E Iron of Two Grain Sizes, Zone-Refined Iron, and Decarburized Iron.

Effect of Interstitial Solutes. — Measurements of the mechanical properties of irradiated Fe (ref. 28), Nb (ref. 29), Mo (ref. 30), and W and Mo (ref. 31) have shown that there is an additional hardening of these metals as a result of postirradiation annealing at about 15% of the absolute melting temperature ($0.15 T_m$), when the irradiation temperature is below this value. It has been suggested that interstitial

²⁸N. E. Hinkle and N. K. Smith, Radiation Metallurgy Section Solid State Division Progress Report for Period Ending January 1967, ORNL-4097, pp. 7-13.

²⁹M. J. Makin and F. J. Minter, Acta Met. 7, 361-366 (1959).

³⁰A. S. Wronski and A. A. Johnson, Phil. Mag. 8, 1067-1070 (1963).

³¹J. Moteff, "Radiation Damage in Body-Centered Cubic Metals and Alloys," p. 727 in Radiation Effects, Gordon and Breach, New York, 1967.

impurities may be contributing to this "radiation-anneal hardening" by interacting with the defects induced by irradiation to produce stronger barriers to dislocation motion. However, none of these measurements were made in studies that used supplemental techniques to determine which interstitial element was involved. Therefore, a detailed investigation³² was begun to determine by suitable techniques which interstitial element contributes to the radiation-anneal hardening in Fe and to obtain an understanding of the mechanism of the interaction between interstitial atoms and defects induced by irradiation. Information gained from this study should be of great value in understanding the radiation hardening and embrittlement of steel.

Barton, Harries, and Mogford³³ observed differences in the magnitude of the radiation effect in steels produced by different methods. They suggested that the variability of the radiation hardening might be associated with the differences in the concentration of interstitial N, which is dependent on the method of steelmaking used (i.e., on the chemistry of the final product). As a result of their work and the fact that the effect of interstitial C on the radiation effect has been extensively studied,³⁴⁻³⁶ we decided to study the effect of interstitial N on radiation effects in Fe.

The starting material for this study was Ferrovac-E Fe (Table 7) swaged from 1 1/4-in.-diam bar to 1/16 in. in diameter and decarburized and denitrogenized in dry H₂ at 800°C for about 96 hr. This material was further swaged and drawn to 0.050 in. in diameter, and pieces were

³²N. E. Hinkle, J. M. Williams, W. E. Brundage, and J. T. Stanley, Radiation Metallurgy Section Solid State Division Progress Report for Period Ending July 1967, ORNL-4195, pp. 15-21.

³³P. J. Barton, D. R. Harries, and I. L. Mogford, J. Iron Steel Inst. (London) 203, 507-510 (1965).

³⁴H. Wagenblast and A. C. Damask, Phys. Chem. Solids 23, 221-227 (1962).

³⁵F. E. Fujita and A. C. Damask, Acta Met. 12, 331-339 (1964).

³⁶J.G.Y. Chow and S. B. McRickard, "Low-Temperature Embrittlement of Iron, Iron Alloys, and Steels by Neutron Irradiations," pp. 120-130 in Flow and Fracture of Metals and Alloys in Nuclear Environments, Am. Soc. Testing Mater. Spec. Tech. Publ. 380, American Society for Testing and Materials, Philadelphia, Pennsylvania, 1965.

cut for resistivity, internal-friction, and tensile specimens. The shoulders of the tensile specimens were fabricated by cold-upsetting the ends of 1 1/2-in.-long wire blanks in a double-ended, hydraulically operated die.

The specimens were heat treated 4 hr in dry H₂ at 700 and 800°C and then cooled in the furnace to establish grain sizes of 30 and 130 μ. Specimens of each grain size were further heat treated at 590°C for 10 hr, quenched in water, and stored in liquid N. In this heat treatment, one group of specimens of each grain size had about 20 ppm N by weight added by treatment in a hydrogen-ammonia atmosphere; a second control group was treated in an atmosphere of pure H₂. These materials are identified as Fe-20N and Fe, respectively. The concentration of N in solid solution was verified by measurements of internal friction. Less than 1 ppm N by weight was detected in the Fe material. The C in solution was below 2 ppm by weight as determined by measurements of internal friction and confirmed by measurements of the magnetic after-effect. However, chemical methods indicated a concentration of 50 to 100 ppm C by weight. Therefore, the C in the Fe and Fe-20N materials is believed to be present in the form of carbides or segregated at grain boundaries, where it makes little contribution to the yield or flow stresses.

As previously reported,³² the neutron irradiations were performed at temperatures between -50 and -100°C in a liquid-nitrogen-cooled cryostat positioned against one side of the ORNL Bulk Shielding Reactor. The neutron flux in this facility was about 3×10^{12} neutrons cm⁻² sec⁻¹ (> 1 Mev). For the results reported below, the specimens were irradiated to a fluence of 4×10^{17} neutrons/cm² (> 1 Mev).

After the irradiation, the assemblies were removed from the irradiation facility without exceeding the irradiation temperature and stored in liquid N for a period of radioactivity decay. Then the assemblies were taken apart in a bath of liquid N and stored in liquid N until testing began. The unirradiated specimens were also stored in liquid N while they awaited testing.

The irradiated specimens were annealed 15 min at temperatures from -36 to 250°C and quenched in liquid N. After this postirradiation anneal, the specimens were tested at -36°C at a strain rate of 0.02 min^{-1} to a strain of 0.04. At given amounts of strain in this range, the strain rate was momentarily changed to 0.002 min^{-1} . Next, the samples were aged for 20 hr at 40°C to permit the complete precipitation of any free nitrogen and carbon interstitials and tensile tested an additional 4% at -36°C according to the same pattern of strain rates. We expected the aging response to be a quantitative measure of the interstitial atoms remaining in solid solution following the postirradiation anneal. In Figs. 19 and 20 we show typical stress-strain curves for the Fe and Fe-20N materials. In these figures, we can observe the

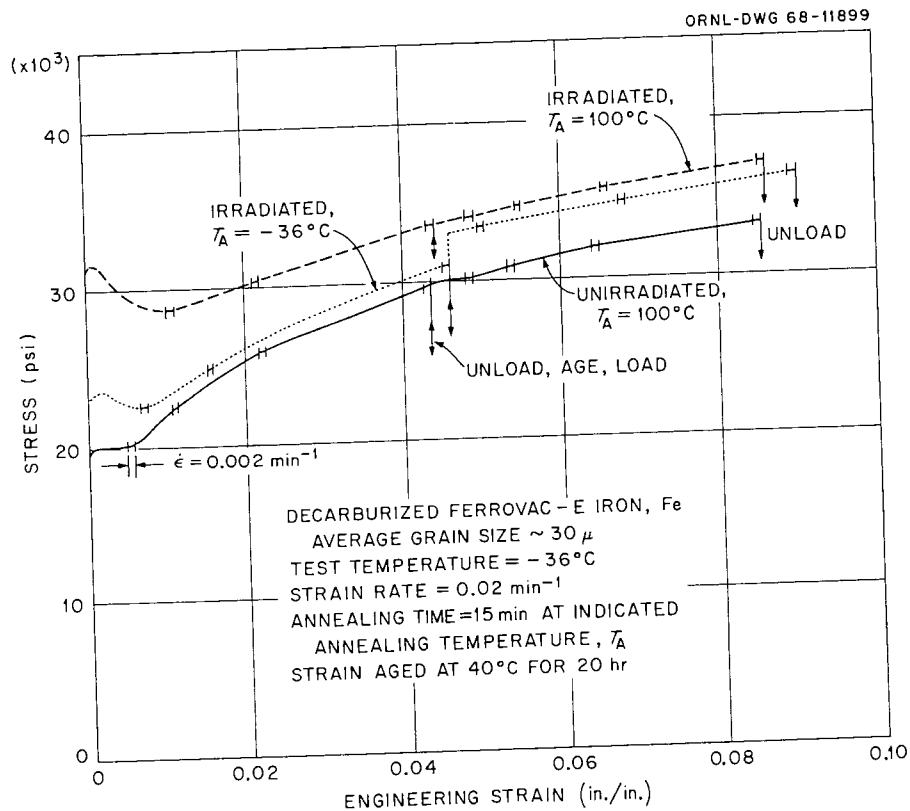


Fig. 19. Stress-Strain Curves at -36°C for Material Fe Showing the Effect of Irradiation, Postirradiation Annealing, and Strain Aging.

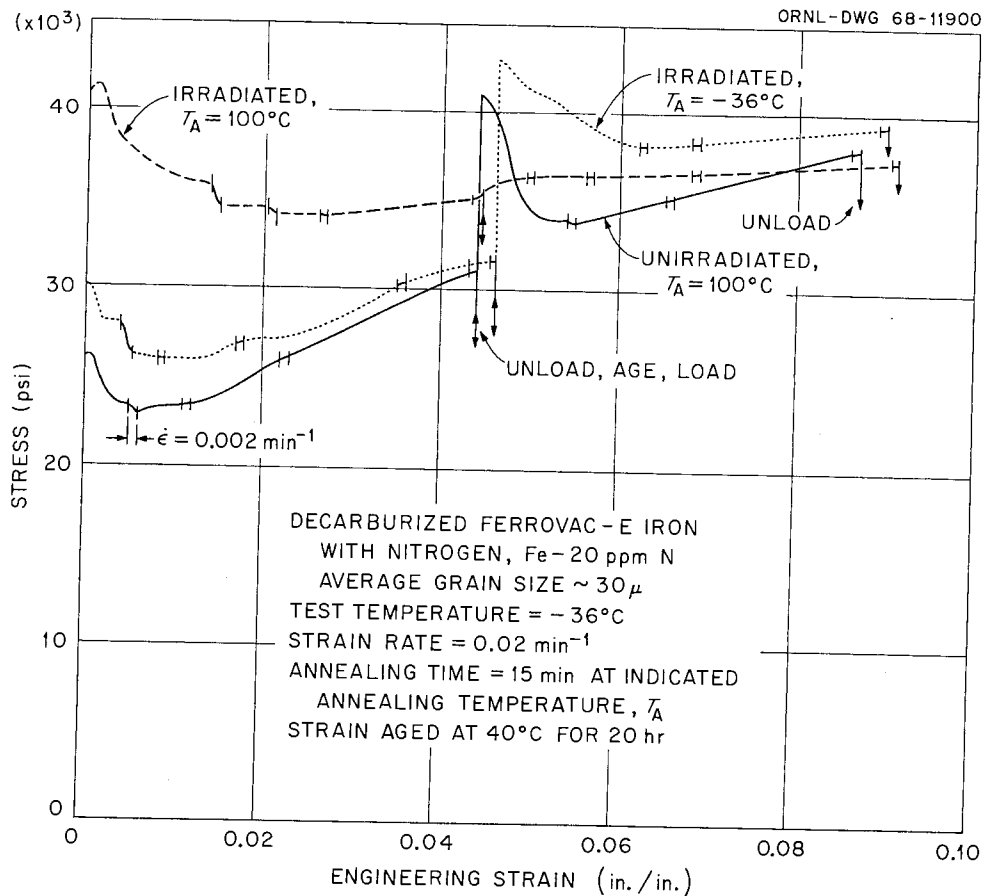


Fig. 20. Stress-Strain Curves at -36°C for Material Fe-20N Showing the Effect of Irradiation, Postirradiation Annealing, and Strain.

increase in yield stress upon irradiation, the radiation-anneal hardening, and the strain aging response. Also indicated are the strains where the strain rate was momentarily decreased to 0.002 min^{-1} .

In Figs. 21 and 22 we show the increase in lower yield stress as a function of postirradiation annealing temperature for fine- and coarse-grained materials. The Fe and Fe-20N of both grain sizes exhibit radiation-anneal hardening which appears to begin at or below 0°C in both grain sizes. In the fine-grained Fe, the radiation-anneal hardening is completed at 100°C , but appears to extend to about 150°C with a slightly greater magnitude for the Fe-20N, as seen in Fig. 21. But the results for the coarse-grained material, shown in Fig. 22, do not indicate any difference in the magnitude or temperature range of

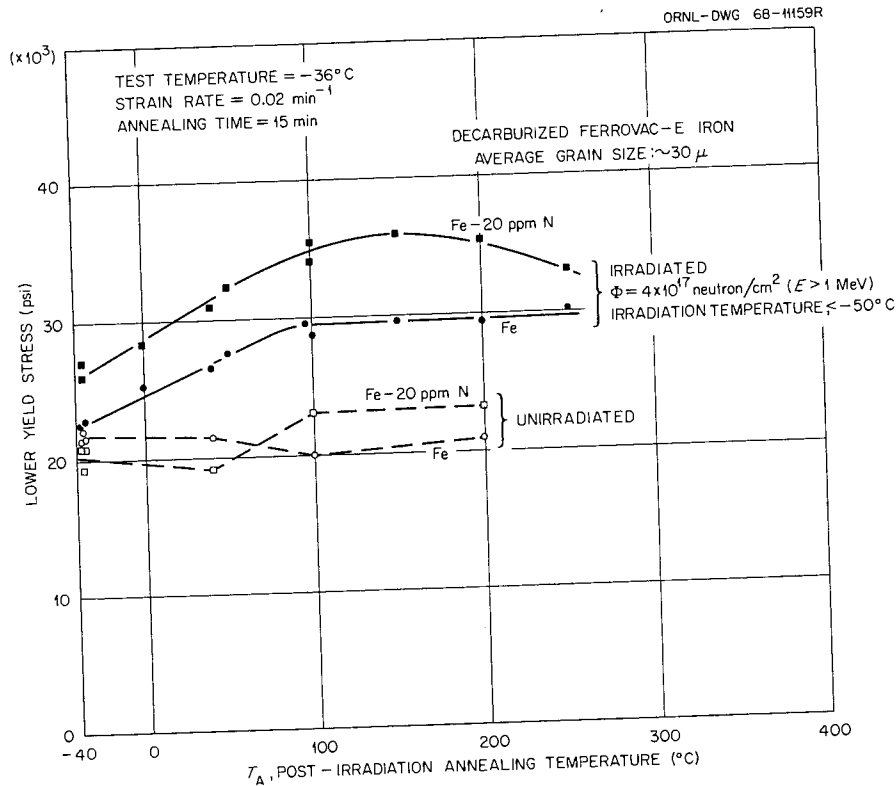


Fig. 21. Effect of Postirradiation Annealing on Separate Tensile Specimens.

the radiation-anneal hardening. There is an indication that softening is beginning at an annealing temperature of 200 to 250°C .

The increase in flow stress upon aging 20 hr at 40°C is shown in Fig. 23 as a function of the postirradiation annealing temperature before aging. The heights of curves in Fig. 23 are a measure of the amounts of interstitial impurities present in solid solution (and therefore able to participate in the strain aging) after the 15-min anneals at temperatures indicated on the abscissa. The most prominent feature in Fig. 23 is the decrease in the aging response of Fe-20N between 0 and 100°C , which reaches a minimum near zero aging response at about 100°C , whereas no minimum is seen for the Fe. The minimum for Fe-20N but not for Fe is also illustrated in Fig. 24, where we show the yield drop after aging the fine-grained materials. Since the magnitude of the yield drop is associated with the concentration of interstitial atoms in solution available to pin dislocation sources,

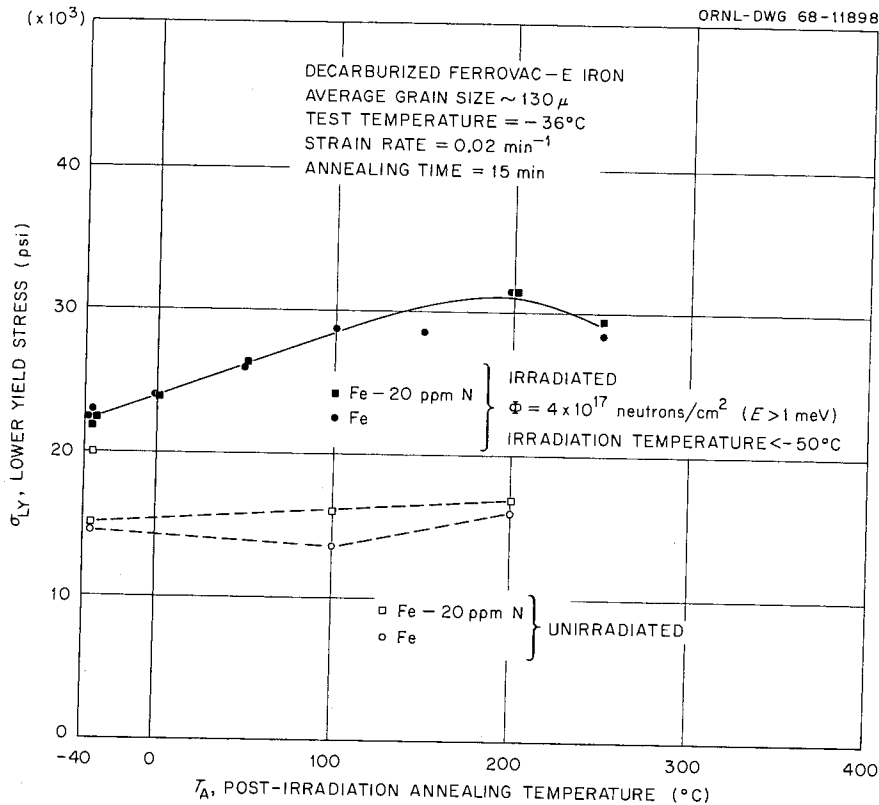


Fig. 22. Effect of Postirradiation Annealing on Separate Tensile Specimens.

the minimum in the aging response in Fig. 23 is evidence again that the N in solution is decreased during the postirradiation anneal at 100°C in Fe-20N. These results are in accord with our previous studies of resistivity and internal friction,³⁷ which indicated an annealing stage of 0 to 100°C in irradiated Fe-20N but no such stage for Fe.

Upon postirradiation annealing above 100°C , the aging response returns in Fe-20N, as shown in Fig. 23 for the flow stress increase upon aging and in Fig. 24 for the yield drop. The previous resistivity measurements³⁷ showed that the resistivity of Fe-20N decreased less than that of Fe in the postirradiation annealing temperature range 100 to 200°C , indicating some return of N to solid solution at these temperatures.

³⁷N. E. Hinkle, J. M. Williams, W. E. Brundage, and J. T. Stanley, Radiation Metallurgy Section Solid State Division Progress Report for Period Ending July 1967, ORNL-4195, pp. 15-21.

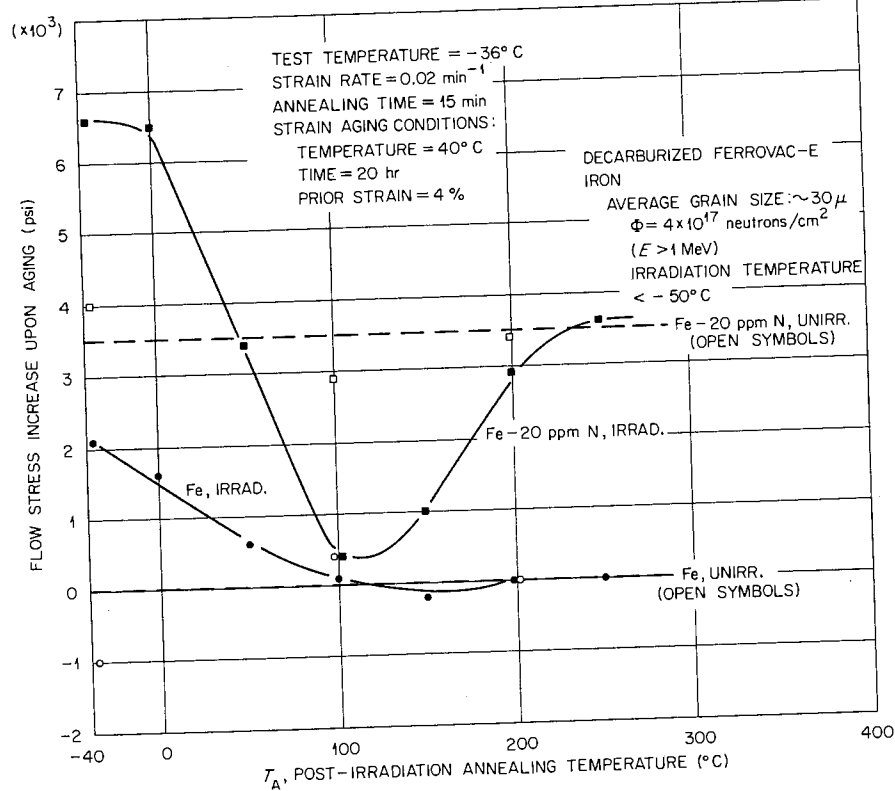


Fig. 23. The Increase in the Flow Stress for Tensile Specimens of Fine-Grain Fe and Fe-20N.

For mild steel irradiated at 45°C , Harries and Little³⁸ showed that the increase in the aging response for the same aging treatment (20 hr at 40°C) occurs at 300 to 400°C .

In comparing Figs. 23 and 24, note an increase in flow stress for the as-irradiated Fe upon aging for 20 hr at 40°C (Fig. 23), but no yield drop (Fig. 24). We believe the increase in flow stress is due to radiation-anneal hardening taking place during the aging treatment. Figure 21 shows that the radiation-anneal hardening of Fe goes to completion at about 100°C . This is consistent with the curve for Fe

³⁸D. R. Harries and E. A. Little, "Effect of Interstitial Nitrogen on Radiation Hardening in Mild Steels," paper presented at ASTM Fourth International Symposium on the Effects of Radiation on Structural Metals held in San Francisco, California, June 26-28, 1968, to be published in the proceedings.

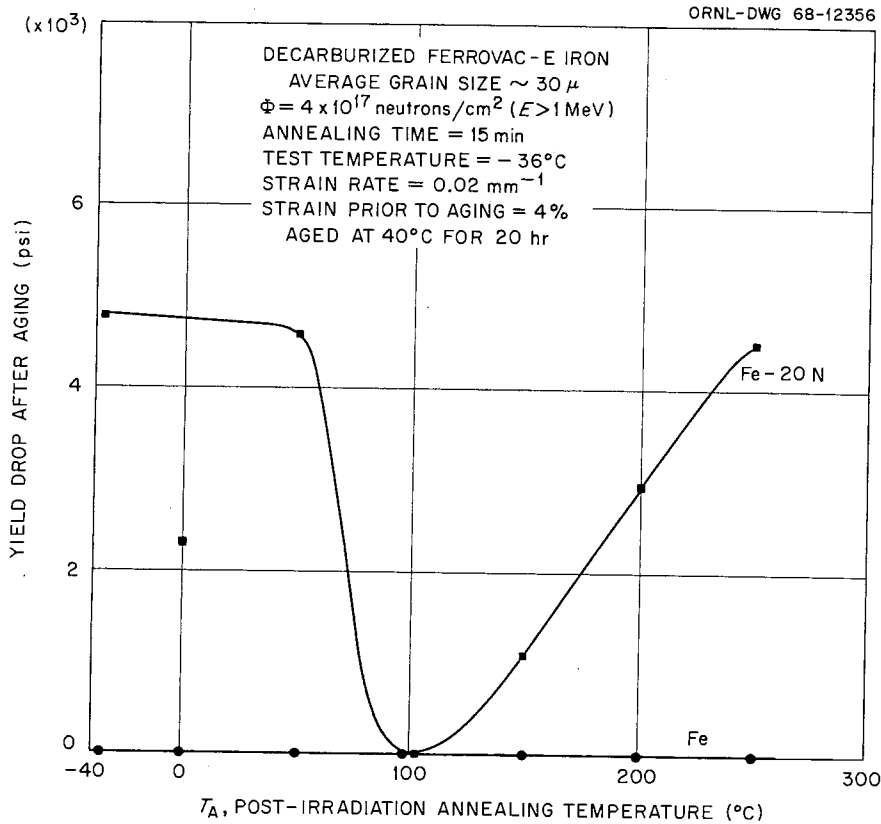


Fig. 24. The Yield Drop Observed for Fine-Grain Fe and Fe-20N after an Aging Treatment of 40°C for 20 hr.

in Fig. 23 in that the flow stress increase upon aging goes to zero for specimens annealed at about 100°C .

The observation that the Fe material exhibits radiation-anneal hardening to only a slightly lesser degree than the Fe-20N material (Fig. 21) suggests that N is not a major contributing factor to the radiation-anneal hardening. On the other hand, the strain aging results (Figs. 23 and 24), supported by earlier studies of resistivity and internal friction,³⁷ show that N is indeed removed from solid solution, presumably at defects produced by the irradiation. Thus, we conclude that the nitrogen-defect complexes do not have a hardening effect. This is further indicated by the recovery to the unirradiated strain aging response for flow stress (Fig. 23) and yield drop (Fig. 24) after annealing to 250°C , whereas the yield stress still exhibits the radiation-anneal-hardened value after annealing to this temperature.

Radiation Effects in Vanadium

Trapping of Interstitial Impurities in Vanadium Defects Produced by Radiation (J. M. Williams, W. E. Brundage, J. T. Stanley)

For the past two years, the Radiation Metallurgy Section has had under way a study of the effect of interstitial impurities on post-irradiation annealing phenomena in refractory metals, particularly Nb (refs. 39-42). The results obtained to date for Nb indicate that annealing effects above room temperature are possibly dominated and at the very least markedly influenced by the interaction of interstitial impurities with defects produced by radiation. In particular, the effects observed so far include (a) segregation of O in solution to radiation-produced dislocation loops in the 100 to 200°C range^{39,40,43} and subsequent return to solution upon annealing at higher temperature^{40,41} and (b) precipitation of C, possibly at dislocation loops.⁴² These effects appear to account for the phenomenon known as "radiation-anneal hardening," first observed by Makin and Minter⁴⁴ in Nb. Indeed, Ohr and Tucker⁴⁵ have found that the anneal hardening is a two-stage process where the lower temperature stage is attributable to O and the higher temperature stage to C.

³⁹J. M. Williams, J. T. Stanley, and W. E. Brundage, Radiation Metallurgy Section Solid State Division Progress Report for Period Ending January 1967, ORNL-4097, pp. 30-41.

⁴⁰J. T. Stanley, J. M. Williams, and W. E. Brundage, Radiation Metallurgy Section Solid State Division Progress Report for Period Ending July 1967, ORNL-4195, pp. 26-34.

⁴¹J. T. Stanley, J. M. Williams, and W. E. Brundage, Radiation Metallurgy Section Solid State Division Progress Report for Period Ending January 1968, ORNL-4246, pp. 42-51.

⁴²J. M. Williams, J. T. Stanley, and W. E. Brundage, Radiation Metallurgy Section Solid State Division Progress Report for Period Ending July 1968, ORNL-4334, pp. 9-20.

⁴³R. Bullough, J. T. Stanley, and J. M. Williams, Metal Sci. J. 2, 93-96 (1968).

⁴⁴M. J. Makin and F. J. Minter, Acta Met. 7, 361-366 (1959).

⁴⁵S. M. Ohr and R. P. Tucker, Radiation Metallurgy Section Solid State Division Progress Report for Period Ending July 1968, ORNL-4334, pp. 29-33.

In view of the fact that V and its alloys are receiving more consideration as potential reactor materials than is Nb, we decided to undertake studies in V to ascertain the extent to which the effects in V parallel those in Nb. Vanadium, like Nb, is a Group VA metal in which the impurities O and N are highly soluble. The solubility of C is quite low. Vanadium, however, has a considerably lower melting point than Nb and is therefore more difficult to purify. Furthermore, C and O move in the same temperature range with nearly the same activation energies.⁴⁶

Sample Preparation. - Two materials labeled VC and VD were used in this study. The starting material for each was 0.032-in.-diam wire obtained from the Materials Research Corporation. The final preparation procedure for each of the materials was an annealing and outgassing treatment by resistive heating of the wires in a high-vacuum bell jar. Material VC was annealed at about 1400°C for about 2.5 hr, and the final vacuum achieved was 6×10^{-9} torr. Material VD was annealed at about 1200°C for about 1 hr, and the final vacuum achieved was 3×10^{-8} torr. Thus, we expected VC to be the purer material. We cut the resulting wires into a number of resistivity and internal-friction samples. The internal-friction samples were 4 in. long, and the resistivity samples were 2 in. long with gage lengths of about 1 in.

Measurement Techniques. - The internal friction was measured using an inverted-torsion pendulum at 1.12 Hz. The resistivity was measured with a thermo-free microvolt potentiometer with the samples immersed in liquid He inside a superconducting solenoid set at 5 kilogauss. The direction of current in the sample was parallel to the magnetic field. Potential contacts to the resistivity samples were made by spot welding 0.005-in.-diam Fe wires to the samples. These contacts were used for the preirradiation measurements but were replaced with platinum contacts before the postirradiation measurements were made. Thus the gage lengths were not precisely constant between the preirradiation and postirradiation measurements. However, the gage lengths were measured as accurately as

⁴⁶R. W. Powers and M. V. Doyle, J. Appl. Phys. 30, 514-524 (1949).

was possible without abusing the samples ($\pm 1\%$) for both sets of potential contacts.

Irradiation Procedures. - The materials VC and VD were irradiated simultaneously in a helium atmosphere in position CP-15 of the ORNL Bulk Shielding Reactor. The temperature of irradiation (60°C) was measured with a thermocouple spot-welded to a dummy sample in the assembly. The neutron fluence was 7×10^{17} neutrons/cm² (≥ 1.0 Mev).

Annealing Procedures. - Internal-friction samples were annealed in place in the torsion pendulum. Resistivity samples were postirradiation annealed by immersing the sample holder in a silicone oil bath, temperature controlled to $\pm 0.2^\circ\text{C}$. Following each anneal, the samples were cooled rather rapidly to room temperature, and the oil was removed simultaneously by immersing them in Freon 11. Then, for the measurement at liquid-helium temperature, the samples were cooled slowly to near liquid-nitrogen temperature by passing cooled nitrogen gas over them and were inserted slowly into the liquid-helium-cooled magnet. This slow-cooling procedure was followed because we found that rapid cooling to liquid-nitrogen temperature seemed to introduce scatter into the data. Westlake⁴⁷ has found resistivity anomalies between measurements at room temperature and at liquid-nitrogen temperature that he attributes to precipitation of H. If H had been introduced into our materials during irradiation, such a phenomenon could possibly account for the sensitivity of our data to the procedural details in this experiment. It should be emphasized, however, that only the apparent scatter in the data and not the main effects reported in our results were affected by the procedures.

Figure 25 shows results from preirradiation measurements of internal friction between 100 and 340°C . The oxygen and nitrogen peaks are identified on the basis of the data of Powers and Doyle.⁴⁶ Table 8 shows the corresponding oxygen and nitrogen concentrations calculated from the data of Powers and Doyle, together with the residual resistivity values for the two materials. The resistivity

⁴⁷D. G. Westlake, Phil. Mag. 16, 905-908 (1967).

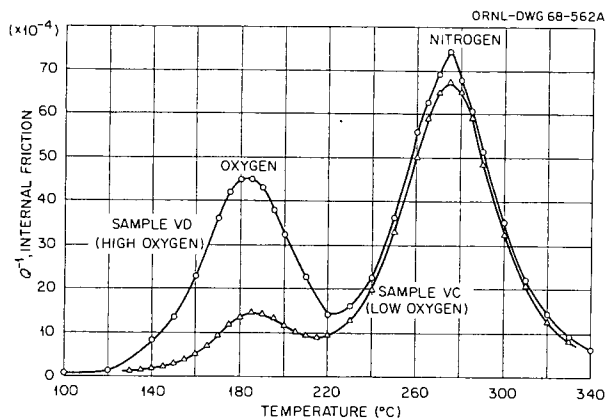


Fig. 25. Internal Friction of Unirradiated Vanadium Materials as a Function of Temperature. Frequency = 1.12 Hz.

Table 8. Characteristics of Vanadium Materials

Material	Concentration, at. ppm		Resistivity ($\mu\Omega$ -cm)
	Oxygen	Nitrogen	
VC	83	1770	1.32 ± 0.02
VD	257	1940	1.59 ± 0.02

values represent the average of measurements on three samples of each material, and the error limits shown probably arise from inconsistencies in the geometrical measurements. We have been unable to locate literature giving the resistivity contributions of interstitial impurities in V, but the resistivity values given in Table 8 are reasonable if it is assumed that the resistivity contributions for O and N are in the range 5 to 10 $\mu\Omega$ -cm/at. %. This range of values is typical of interstitial impurities in body-centered cubic metals. If the resistivity difference of 0.27 $\mu\Omega$ -cm between the two samples is attributed to the interstitial impurity difference of 344 ppm (atomic), we get a resistivity of 7.8 $\mu\Omega$ -cm/at. % interstitial impurities, making no distinction between O and N as to effect on resistivity.

After irradiation, an internal-friction sample from material VD was annealed first at the oxygen-peak temperature (185°C) and then at the nitrogen-peak temperature (275°C), and internal friction was measured as a function of time at the two temperatures. Figure 26

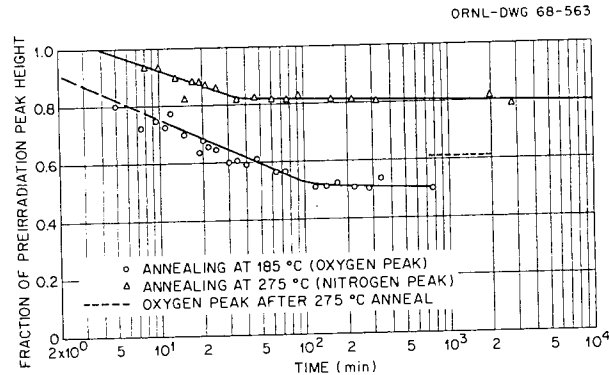


Fig. 26. Fractional Decrease of Internal-Friction Peaks Due to Oxygen and Nitrogen in Vanadium Material VD as a Function of Annealing Time at the Peak Temperatures.

shows the results of this experiment. The oxygen peak had decreased by about 50% after 100 min annealing at 185°C. The nitrogen peak decreased about 20% during the anneal at 275°C. After the anneal at 275°C, the sample was returned to 185°C, and some recovery of the decrease in the oxygen peak was noted.

Figure 27 shows results of postirradiation isochronal annealing for materials VC and VD over the range 60 to 220°C. The change in resistivity is taken with respect to the unirradiated resistivity. Thus the samples increased in resistivity by about 0.035 $\mu\Omega$ -cm upon irradiation and decreased as shown in the figure upon isochronal annealing.

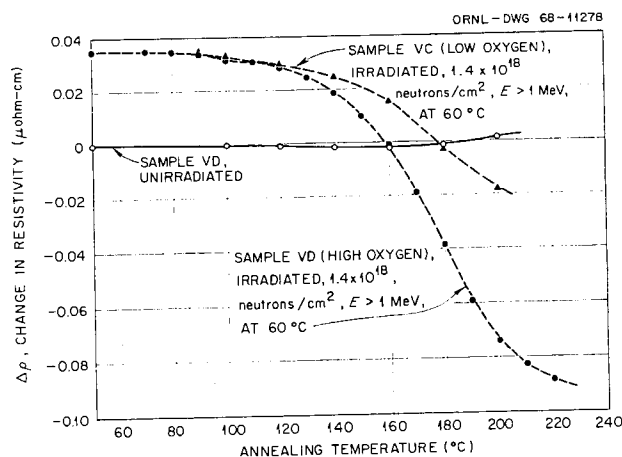


Fig. 27. Changes in Resistivity of Vanadium upon Isochronal Annealing. Materials VD-irradiated and VC-irradiated were annealed for 1-hr periods at 20°C intervals.

However, since the gage lengths were not precisely the same for the pre-irradiation and postirradiation measurements, an explanation of the way in which we arrived at the increase of $0.035 \mu\Omega\text{-cm}$ is needed. For four samples (two each of VC and VD) the resistivity increase upon irradiation was found to range from 0.025 to $0.049 \mu\Omega\text{-cm}$ with an average of $0.035 \mu\Omega\text{-cm}$, and these measurements included the error associated with changing and remeasuring the gage length. Thus, for purposes of presenting the magnitudes of the effects in these samples on some absolute basis, we assumed the resistivity increased by $0.035 \mu\Omega\text{-cm}$ upon irradiation in all the samples. The principal feature illustrated in Fig. 27 is that both materials exhibit a large decrease in resistivity between 100 and 200°C , but the decrease is much smaller in material VC (low oxygen content) than in VD (high oxygen content). Furthermore, the resistivity goes below the preirradiation value. In view of the problem of gage length, we would not argue that the appearance of going below the preirradiation value is necessarily real in material VC, but it decidedly is real in VD. Unirradiated material VD exhibits a slight decrease in resistivity up to 140°C and thereafter increases slightly. This increase appears to be reversible. The resistivity decreases again when we return the sample to 140°C after annealing it at 200°C . However, the magnitudes of the effects in unirradiated VD are much smaller than in the irradiated material.

The data represented as 1-hr isochronal annealing data in Fig. 27 are in fact the end points of a series of 1-hr isothermal anneals on one sample at successively increasing temperatures, where measurements were made as a function of time during the 1-hr period. From this type of measurement, the activation energy of the process can be determined from the change in slope attendant upon changing the temperature abruptly from T_1 to T_2 . Figure 28 shows the series of isothermal anneals obtained on VC. The activation energies that were calculated from the changes in slope are tabulated in Table 9. It is difficult to estimate the error in this method of determining activation energy, but by drawing various curves through the data in Fig. 28, we estimate that the scatter in the data warrants assignment of an error band no greater

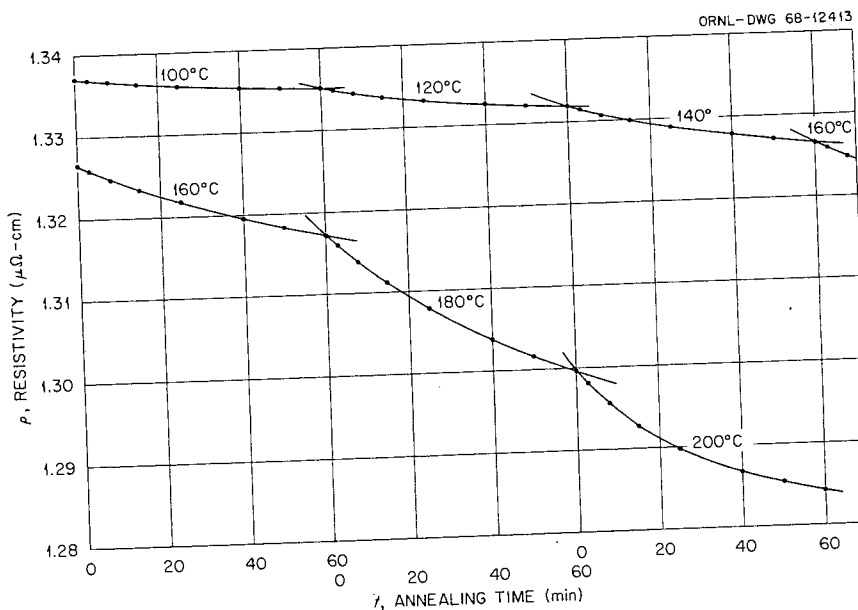


Fig. 28. Resistivity as a Function of Annealing Time at Successively Increasing Temperatures in an Irradiated Sample of Vanadium Material VC.

Table 9. Activation Energies Obtained from Ratio-of-Slopes Method

Annealing Temperatures, °C		E_m Activation Energy (ev)
T_1	T_2	
100	120	1.23
120	140	1.24
140	160	1.14
160	180	1.32
180	200	1.02

than ± 0.12 ev to any one determination, assuming all the apparent scatter is indeed random. The values are in reasonably good agreement except for the value 1.02 ev obtained for the last temperature transition from 180 to 200°C. In Nb, it has been found that the apparent activation energy for Stage III falls off as the measurements are made at higher

temperatures.^{48,49} This is attributed to the concept that the saturation value is strongly temperature dependent, a circumstance that would invalidate most methods of determining activation energy as saturation is approached.

We shall first discuss the annealing effects between 100 and 220°C, but before proceeding, perhaps some background information on previous annealing studies in this temperature region in body-centered cubic metals will help facilitate discussion. Pronounced resistivity annealing stages in this temperature region have been observed in both neutron-irradiated and deformed body-centered cubic metals,⁵⁰⁻⁵³ and because irradiation is known to produce point defects, these stages were first attributed to annealing of point defects and called Stage III annealing. Now, however, there is mounting evidence that in the Group VA metals these resistivity decreases are caused by the migration of interstitial impurities to defect structures produced by irradiation or deformation. The evidence that this is the case in Nb and Ta appears quite conclusive.^{48,49,54,55} Earlier, Köthe and Schlät⁵⁶ observed that the

⁴⁸J. M. Williams, J. T. Stanley, and W. E. Brundage, Metal Sci. J. 2, 100-104 (1968).

⁴⁹A. Köthe, Acta Met. 16, 357-367 (1968).

⁵⁰D. E. Peacock and A. A. Johnson, Phil. Mag. 8, 563-577 (1963).

⁵¹J. Moteff and J. P. Smith, "Recovery of Defects in Neutron-Irradiated Tungsten," pp. 171-187 in Flow and Fracture of Metals and Alloys in Nuclear Environments, Am. Soc. Testing Mater. Spec. Tech. Publ. 380, American Society for Testing and Materials, Philadelphia, Pennsylvania, 1965.

⁵²D. G. Martin, Acta Met. 5, 371-376 (1957).

⁵³L. Stals and J. Nihoul, Phys. Status Solidi 8, 785-793 (1965).

⁵⁴R. Bullough, J. T. Stanley, and J. M. Williams, Metal Sci. J. 2, 93-96 (1968).

⁵⁵Z. C. Szkopiak and B. Pouzet, "Effect of Oxygen on 'Stage III' Recovery in Cold-Worked Niobium," pp. 709-723 in International Conference on Vacancies and Interstitials in Metals, Vol. II, Jülich, Germany, September 1968.

⁵⁶A. Köthe and F. Schlät, J. Mater. Sci. 2, 201-205 (1967).

magnitude of the annealing effects in deformed V decreased with decreasing oxygen content and concluded that effects in V are analogous to those in Nb and Ta. This interpretation has recently been questioned by Perepezko *et al.*⁵⁷ on the basis of an activation energy determination. These workers observed annealing effects between 100 and 200°C in both deformed and neutron-irradiated V that closely resemble those of Köthe and Schlät in deformed material and those of the present work in irradiated material. Perepezko *et al.*⁵⁷ measured activation energies of 0.87 ± 0.07 ev and 0.79 ± 0.09 ev for the annealing stage in deformed and irradiated materials, respectively. Since these activation energies are lower than the diffusion activation energies of either C, O, or N and greater than the diffusion activation energy of H, they conclude that the annealing stage should be attributed to annealing of lattice vacancies, possibly to impurity traps. It would appear that the activation energies of about 0.8 ev are somewhat lower than is usually measured for an annealing process in this temperature region; as the authors point out,⁵⁷ an enormous number of jumps (about 10^8) of the migrating species is implied.

In view of the considerably larger activation energy measured in the present experiment, we submit that the mechanism of migration of interstitial impurities to radiation-produced defects, probably dislocation loops, still provides a simple and satisfactory explanation of events in this temperature region. First of all, the effect takes place in the temperature region where internal-friction measurements indicate O first becomes highly mobile, whether it migrates to radiation-produced defects or not. Thus, we prefer to attribute the internal-friction decrease at the oxygen-peak temperature to migration of O to some site where it is effectively removed from interstitial solid solution. This interpretation and the notion that the resistivity decrease is connected with the internal-friction decrease are supported by the fact that the activation energy for the resistivity decrease measured in this experiment (Table 9) agrees with the diffusion activation energy of O (1.25 ev) (ref. 58).

⁵⁷J. H. Perepezko, R. F. Murphy, and A. A. Johnson, "Point Defects in Vanadium." To be published in The Philosophical Magazine.

⁵⁸R. W. Powers and M. V. Doyle, J. Appl. Phys. 30, 514-524 (1949).

The magnitude of the resistivity decrease and the fact that the resistivity drops below the preirradiation value are readily accounted for on the basis of this mechanism. The internal-friction decrease (Fig. 26) indicates that about 50% of the O or 130 ppm (atomic) is removed from solution in material VD. The magnitude of the resistivity decrease for this material, $0.125 \mu\Omega\text{-cm}$, divided by the above-mentioned figure, $7.8 \mu\Omega\text{-cm at. } \%$, would suggest removal of about 160 ppm (atomic), which is basically in good agreement considering that the figure $7.8 \mu\Omega\text{-cm at. } \%$ represents about an average of the resistivity contributions of O and N rather than the contribution of O specifically. Since most of the residual resistivity is caused by interstitial impurities, any effect involving a sizable fraction of these impurities is likely to override the relatively small increase in resistivity caused by irradiation. It is to be expected that material containing less O will exhibit a smaller resistivity decrease, as was the case in this experiment (Fig. 27).

Resistivity annealing studies were not made above 220°C , but the fact that the nitrogen peak decreases with time at the nitrogen-peak temperature (275°C) indicates that the behavior of N is similar to that of O and that a large resistivity decrease should be expected in this temperature region as well. Köthe and Schlät observed such a resistivity decrease centered at 265°C in deformed V containing 1000 ppm N (ref. 56).

In the discussion so far we have ignored possible effects due to C, but because the diffusion activation energy for C (1.18 ev) is only slightly lower than that for O (1.26 ev), involvement of C in the annealing effect below 200°C cannot be ruled out. The width of the 100 to 200°C annealing stage in V is somewhat greater than the corresponding stage in Nb (ref. 59), and this suggests that the effect might involve the migration of both O and C. However, the solubility of C in equilibrium solid solution in V is thought to be quite low, and the absence of

⁵⁹J. T. Stanley, J. M. Williams, and W. E. Brundage, Radiation Metallurgy Section Solid State Division Progress Report for Period Ending July 1967, ORNL-4195, pp. 26-34.

any major resistivity decrease upon annealing in the unirradiated V (Fig. 27) shows that almost all the C is in equilibrium before irradiation. Furthermore, the 182°C internal-friction peak (Fig. 25) is stable and fairly narrow, suggesting a single relaxation due to O alone.

ORNL-4369
UC-25 - Metals, Ceramics, and Materials

INTERNAL DISTRIBUTION

- | | | | |
|-------|-------------------------------|------|----------------------------------|
| 1-3. | Central Research Library | 68. | R. R. Coltman |
| 4-5. | ORNL - Y-12 Technical Library | 69. | W. D. Compton (consultant) |
| | Document Reference Section | 70. | T. F. Connolly |
| 6-25. | Laboratory Records Department | 71. | J. H. Coobs |
| 26. | Laboratory Records, ORNL R.C. | 72. | J. A. Cox |
| 27. | ORNL Patent Office | 73. | J. H. Crawford, Jr. (consultant) |
| 28. | M. M. Abraham | 74. | J. C. Crump |
| 29. | G. M. Adamson, Jr. | 75. | F. L. Culler |
| 30. | L. G. Alexander | 76. | J. E. Cunningham |
| 31. | R. W. Armstrong (consultant) | 77. | G. V. Czjzek |
| 32. | W. E. Atkinson | 78. | J. H. DeVan |
| 33. | Robert Bakish (consultant) | 79. | G. W. Flack |
| 34. | T. O. Baldwin | 80. | J. L. Fowler |
| 35. | J. H. Barrett | 81. | A. P. Fraas |
| 36. | S. E. Beall | 82. | J. H. Frye, Jr. |
| 37. | R. J. Beaver | 83. | J. L. Gabbard |
| 38. | P. R. Bell | 84. | W. B. Gauster |
| 39. | M. Bender | 85. | H. A. Gersch (consultant) |
| 40. | W. T. Berg | 86. | J. H. Gillette |
| 41. | R. G. Berggren | 87. | J. J. Gilman (consultant) |
| 42. | Carla Bertocci (consultant) | 88. | R. J. Gray |
| 43. | U. Bertocci | 89. | W. R. Grimes |
| 44. | J. O. Betterton, Jr. | 90. | H. D. Guberman |
| 45. | D. S. Billington | 91. | J. P. Hammond |
| 46. | H. Birnbaum (consultant) | 92. | W. O. Harms |
| 47. | A. L. Boch | 93. | C. S. Harrill |
| 48. | E. G. Bohlmann | 94. | M. R. Hill |
| 49. | E. D. Bolling | 95. | N. E. Hinkle |
| 50. | E. S. Bomar | 96. | D. K. Holmes |
| 51. | B. S. Borie | 97. | A. S. Householder |
| 52. | C. J. Borkowski | 98. | J. P. Howe (consultant) |
| 53. | G. E. Boyd | 99. | A. P. Huber (K-25) |
| 54. | M. A. Breazeale (consultant) | 100. | L. D. Hulett |
| 55. | M. A. Bredig | 101. | H. Inouye |
| 56. | R. B. Briggs | 102. | L. H. Jenkins |
| 57. | F. R. Bruce | 103. | R. J. Jones |
| 58. | W. E. Brundage | 104. | W. H. Jordan |
| 59. | C. T. Butler | 105. | G. W. Keilholtz |
| 60. | N. Cabrera (consultant) | 106. | M. T. Kelley |
| 61. | J. W. Cable | 107. | R. H. Kernohan |
| 62. | J. V. Cathcart | 108. | R. F. Kimball |
| 63. | Y. Chen | 109. | E. M. King |
| 64. | H. R. Child | 110. | C. E. Klabunde |
| 65. | G. W. Clark | 111. | F. A. Kocur |
| 66. | J. W. Cleland | 112. | J. S. Koehler (consultant) |
| 67. | A. M. Clogston (consultant) | 113. | W. C. Koehler |

- | | | | |
|------|------------------------------|----------|-----------------------------|
| 114. | R. B. Korsmeyer | 153. | O. Sisman |
| 115. | J. A. Krumhansl (consultant) | 154. | G. M. Slaughter |
| 116. | J. A. Lane | 155. | L. Slifkin |
| 117. | C. E. Larson | 156. | G. P. Smith |
| 118. | G. Leibfried (consultant) | 157. | H. G. Smith |
| 119. | A. B. Lewis | 158. | A. H. Snell |
| 120. | R. S. Livingston | 159. | E. Sonder |
| 121. | A. L. Lotts | 160. | A. L. Southern |
| 122. | T. S. Lundy | 161. | F. Specht |
| 123. | H. G. MacPherson | 162. | J. O. Stiegler |
| 124. | R. W. McClung | 163. | W. J. Stelzman |
| 125. | H. C. McCurdy | 164. | B. G. Streetman |
| 126. | D. L. McElroy | 165. | E. H. Taylor |
| 127. | C. J. McHargue | 166. | A. S. Tetelman (consultant) |
| 128. | A. J. Miller | 167. | G. T. Trammell (consultant) |
| 129. | E. C. Miller | 168. | D. B. Trauger |
| 130. | J. W. Mitchell (consultant) | 169. | David Turnbull (consultant) |
| 131. | H. A. Mook | 170. | H. A. Ullmaier |
| 132. | R. M. Moon, Jr. | 171. | C. C. Webster |
| 133. | K. Z. Morgan | 172-272. | M. S. Wechsler |
| 134. | C. M. Nelson (consultant) | 273. | R. A. Weeks |
| 135. | R. M. Nicklow | 274. | A. M. Weinberg |
| 136. | T. S. Noggle | 275. | J. R. Weir, Jr. |
| 137. | A. S. Nowick (consultant) | 276. | R. D. Westbrook |
| 138. | O. S. Oen | 277. | G. D. Whitman |
| 139. | S. M. Ohr | 278. | E. P. Wigner (consultant) |
| 140. | A. R. Olsen | 279. | M. K. Wilkinson |
| 141. | V. Pare | 280. | F. E. Williams (consultant) |
| 142. | P. Patriarca | 281. | G. C. Williams |
| 143. | J. C. Pigg | 282. | J. M. Williams |
| 144. | H. Pomerance | 283. | R. O. Williams |
| 145. | L. J. Raubenheimer | 284. | W. R. Willis (consultant) |
| 146. | R. E. Reed | 285. | J. C. Wilson |
| 147. | M. T. Robinson | 286. | E. O. Wollan |
| 148. | J. L. Scott | 287. | R. F. Wood |
| 149. | S. T. Sekula | 288. | H. L. Yakel |
| 150. | E. D. Shipley | 289. | F. W. Young, Jr. |
| 151. | W. A. Sibley | 290. | Gale Young |
| 152. | R. H. Silsbee (consultant) | | |

EXTERNAL DISTRIBUTION

291. S. Amelinckx, Solid State Physics Department, C.E.N., Mol-Donk, Belgium
292. P. Baruch, Laboratoire de Physique, Ecole Normale Supérieure, Paris V, France
293. V. B. Bhanot, Physics Department, Panjab University, Chandigarh-3, India
294. T. H. Blewitt, Argonne National Laboratory

295. R. O. Bolt, California Research Corporation, Richmond, Calif.
296. J. A. Brinkman, Science Center, Aerospace and Systems Group, North American Rockwell Corporation, 1049 Camino Dos Rios, Thousand Oaks, California 91360
297. H. Brooks, 217 Pierce Hall, Harvard University, Cambridge, Massachusetts 02138
298. J. G. Castle, Jr., Physics Department, Westinghouse Electric Corp., Research Laboratories, Pittsburgh, Pennsylvania
299. E. D. Clavert, U. S. Bureau of Mines, P. O. Box 492, Albany, Oregon
300. C. B. Cooper, Department of Physics, University of Delaware, Newark, Delaware
- 301-302. D. F. Cope, RDT Site Office (Oak Ridge National Laboratory)
303. D. Dautreppe, Head, Solid State Physics, Centre D'Etude Nucleaires de Grenoble, P. O. Box 269, Grenoble, France
304. J. Diehl, Max-Planck-Institut für Metallforschung, Institut für Sondermetalle, Seestrasse 92, 7000 Stuttgart 1, Germany
305. H. D. Dietz, Lehrstuhl für Reaktorwerkstoffe, Technische Hochschule, Aachen, Germany
306. L. B. Emlet, Union Carbide Corporation, New York
307. N. Engel, Chemical Engineering Department, Georgia Institute of Technology, 225 North Avenue, N. W., Atlanta, Georgia 30332
308. H. Y. Fan, Solid State Physics Department, Purdue University, Lafayette, Indiana
309. H. B. Finger, Atomic Energy Commission, Washington
310. J. Friedel, Physique des Solides, Faculte des Sciences d'Orsay, Orsay, France
311. Angelo Giambusso, Atomic Energy Commission, Washington
312. R. G. Gilliland, Department of Chemical Engineering, Massachusetts Institute of Technology, 77 Massachusetts Avenue, Cambridge, Massachusetts 02139
313. R. H. Gillette, European Research Associates, Brussels, Belgium
314. W. W. Grigorieff, Assistant to the Executive Director, Oak Ridge Associated Universities
315. R. F. Hehemann, Case Western Reserve, Department of Metallurgy, University Circle, Cleveland, Ohio 44106
316. J. Hitch, Office of Isotope Development, AEC, Washington
317. E. E. Hoffman, General Electric, Cincinnati, Ohio
318. J. R. Hunter, Reactor Vessels Branch, Division of Reactor Development and Technology, AEC, Washington
319. H. Huntington, Department of Physics, Rensselaer Polytechnic Institute, Troy, New York
320. J. R. Johnson, Minnesota Mining and Manufacturing Company, St. Paul, Minnesota
321. L. K. Keys, Principal Engineer, Radiation Effects to Metals, Nuclear Materials and Propulsion Operation, General Electric Co., Cincinnati, Ohio 45215
322. C. Kikuchi, University of Michigan, Willow Run Laboratory, Ann Arbor, Michigan
- 323-324. W. J. Larkin, Atomic Energy Commission, Oak Ridge

325. Benjamin Lax, Lincoln Laboratory, Lexington, Massachusetts
 326. C. Lehmann, KFA-Werkstoffinstitut, Jülich, Germany
 327. R. I. Leininger, Battelle Memorial Institute, 505 King Avenue,
 Columbus, Ohio 43201
 328. A. B. Lidiard, AERE, Harwell, England
 329. J. J. Lombardo, NASA, Lewis Research Center
 330. W. M. Lomer, AERE, Harwell, England
 331. W. C. Mallard, Department of Physics, Emory University,
 Atlanta, Georgia
 332. W. D. Manly, Union Carbide Corporation, Stellite Division
 333. W. Marshall, AERE, Harwell, England
 334. R. S. Mateer, Department of Metallurgy, University of Kentucky,
 Lexington, Kentucky
 335. P. W. McDaniel, Division of Research, USAEC, Washington
 336. A. Merlini, Solid State Physics Department, C.C.R.-EURATOM,
 Ispra (Varese), Italy
 337. R. M. Milton, Linde Division, Union Carbide Corporation, P. O.
 Box 44, Tonawanda, New York
 338. R. R. Nash, NASA, Washington
 339. E. F. Nippes, Rensselaer Polytechnic Institute, Troy, N. Y.
 340. R. E. Pahler, Atomic Energy Commission, Washington
 341. R. M. Parke, MAB, National Academy of Science, Washington
 342. J. Pheline, Centre d'Etudes Nucleaires de Saclay, Paris, France
 343. J. M. Prosser, Atomic Energy Commission, Washington
 344. H. B. Rahner, Savannah River Operations
 345. R. E. Reed-Hill, Department of Metallurgy, University of Florida,
 Gainesville, Florida 32601
 346. Research and Development Division, AEC, ORO
 347. F. N. Rhines, Department of Metallurgy, University of Florida,
 Gainesville, Florida 32601
 348. A. E. Ruark, Atomic Energy Commission, Washington
 349. H. Saito, Department of Physics, College of General Education,
 Osaka University, Osaka, Japan
 350. R. W. Schroeder, NASA, Lewis Research Center
 351. R. J. Schuttler, Service SEPP, CEN/FAR (Ford de Chatillion),
 Boite Postale 6, Fontenay-aux-Roses (Seine), France
 352. F. C. Schwenk, Atomic Energy Commission, Washington
 353. A. Seeger, Max-Planck-Institut für Metallforschung, Institut für
 Physik, Azenbergstrasse 12, 7000 Stuttgart 1, Germany
 354. W. W. Shaver, Corning Glass Works, Corning, New York
 355. A. A. Shoudy, Atomic Power Development Associate, Inc.
 356. J. M. Simmons, Division of Reactor Development, AEC, Washington
 357. O. C. Simpson, Argonne National Laboratory
 358. E. E. Sinclair, Atomic Energy Commission, Washington
 359. E. E. Stansbury, Chemical and Metallurgical Engineering Depart-
 ment, University of Tennessee, Knoxville, Tennessee 37916
 360. D. K. Stevens, Materials and Metallurgy Branch, AEC, Washington
 361. G. L. Stiehl, Convair Division of General Dynamics Corporation,
 San Diego, California
 362. R. Street, Department of Physics, Monash University, P. O. Box
 92, Clayton, Victoria, Australia

363. J. A. Swartout, 270 Park Avenue, New York, New York
364. D. O. Thompson, Science Center, Aerospace and Systems Group, North American Rockwell Corp., 1049 Camino Dos Rios, Thousand Oaks, California 91360
365. J. B. Trice, Military Space Vehicle Department, General Electric Company, Philadelphia, Pennsylvania
366. R. P. Tucker, Max-Planck-Institut für Metallforschung, Institut für Sondermetalle, Seestrasse 92, 7000 Stuttgart 1, Germany
367. T. J. Turner, Department of Physics, Wake Forest College, Winston-Salem, North Carolina
368. A. Van Echo, Atomic Energy Commission, Washington
369. G. H. Vineyard, Brookhaven National Laboratory, Upton, Long Island, New York
370. G. D. Watkins, General Electric Research Laboratories, Schenectady, New York
371. J. Weertman, Materials Science Department, Technological Institute, Northwestern University, Evanston, Illinois 60201
372. G. W. Wench, Atomic Energy Commission, Washington
373. Westinghouse Electric Corporation, Research Laboratories, Pittsburgh, Pennsylvania
374. M. J. Whitman, Atomic Energy Commission, Washington
375. C. H. T. Wilkins, Metallurgical Engineering Department, University of Alabama, P. O. Box G, Tuscaloosa, Alabama 35486
376. Manfred Wuttig, Metallurgy Department, University of Missouri at Rolla, Rolla, Missouri 65401
377. R. A. Young, Engineering Experiment Station, Georgia Institute of Technology, Atlanta, Georgia 30332
378. C. D. Yost, ARPA, Pentagon, Washington, D. C.
379. Laboratory and University Division, AEC, ORO
- 380-599. Given distribution as shown in TID-4500 under Metals, Ceramics, and Materials category (25 copies - CFSTI)